

Gradient-preserving hyper-reduction of nonlinear dynamical systems via discrete empirical interpolation

Cecilia Pagliantini* and Federico Vismara†

Abstract

This work proposes a hyper-reduction method for nonlinear parametric dynamical systems characterized by gradient fields such as (port-)Hamiltonian systems and gradient flows. The gradient structure is associated with conservation of invariants or with dissipation and hence plays a crucial role in the description of the physical properties of the system. Traditional hyper-reduction of nonlinear gradient fields yields efficient approximations that, however, lack the gradient structure. We focus on Hamiltonian gradients and we propose to first decompose the nonlinear part of the Hamiltonian, mapped into a suitable reduced space, into the sum of d terms, each characterized by a sparse dependence on the system state. Then, the hyper-reduced approximation is obtained via discrete empirical interpolation (DEIM) of the Jacobian of the derived d -valued nonlinear function. The resulting hyper-reduced model retains the gradient structure and its computationally complexity is independent of the size of the full model. Moreover, *a priori* error estimates show that the hyper-reduced model converges to the reduced model and the Hamiltonian is asymptotically preserved. Whenever the nonlinear Hamiltonian gradient is not globally reducible, i.e. its evolution requires high-dimensional DEIM approximation spaces, an adaptive strategy is performed. This consists in updating the hyper-reduced Hamiltonian via a low-rank correction of the DEIM basis. Numerical tests demonstrate the applicability of the proposed approach to general nonlinear operators and runtime speedups compared to the full and the reduced models.

1 Introduction

We consider large-scale parametric dynamical systems where the velocity describing the flow is characterized by nonlinear gradient fields. These are problems of the form

$$\dot{y}(t, \eta) = X(y(t, \eta), \eta) \quad \text{for } t \geq t_0, \quad (1.1)$$

where $\eta \in \mathbb{R}^p$, $p \geq 1$, is a parameter, $y : (t_0, \infty) \times \mathbb{R}^p \rightarrow \mathbb{R}^n$ is the state variable, and the velocity field $X : \mathbb{R}^n \times \mathbb{R}^p \rightarrow \mathbb{R}^n$ is assumed to be of the form $X(y, \eta) = S \nabla_y \mathcal{H}(y, \eta)$, with $S \in \mathbb{R}^{n \times n}$ and \mathcal{H} a nonlinear function of the state. Examples of such dynamical systems are gradient flows, where S is a negative semi-definite matrix, or Hamiltonian systems, in which case S is skew-symmetric. The gradient structure of the velocity field X plays a crucial role in the characterization of the dynamics and of the physical properties of the system since it is associated with dissipation or preservation of quantities such as energy or entropy.

In this work we focus on Hamiltonian dynamical systems and the goal is to develop numerical approximation methods for their efficient solution in large-scale scenarios, i.e. when the number n of

*Centre for Analysis, Scientific computing and Applications, Eindhoven University of Technology (TU/e), The Netherlands. Email: c.pagliantini@tue.nl

†Centre for Analysis, Scientific computing and Applications, Eindhoven University of Technology (TU/e), The Netherlands. Email: f.vismara@tue.nl

degrees of freedom is high, and for many instances of the parameter. A major challenge in this task is to preserve the physical properties of the dynamics and, in particular, the Hamiltonian gradient structure of the velocity field.

In the context of large-scale many-query simulations of parametric differential problems, model order reduction (MOR) and reduced basis methods (RBM) have been developed to provide efficient high-fidelity surrogate models on lower-dimensional spaces where the bulk of the dynamics takes place. Their success notwithstanding, the application of RBM to problems of the form (1.1) might lead to unstable and qualitatively wrong solution behavior since the gradient structure of the model can be destroyed during dimension reduction. To address this issue in solving Hamiltonian systems, structure-preserving MOR techniques have been developed in recent years to derive reduced models that retain (at least part of) the geometric structure underlying the dynamics [17, 4, 22, 1, 3, 11, 15]. Although these methods have led to the successful construction of stable low-dimensional models, little attention has been paid to the efficient treatment of nonlinear operators. Indeed, in the presence of Hamiltonian functions with general nonlinear dependence on the state, the computational cost of solving the reduced model might still depend on the size of the underlying full model, resulting in simulation times that hardly improve over the original system simulation. This is a well-known issue in model order reduction and has led to the so-called hyper-reduction methods. These usually approximate the high-dimensional nonlinear operators using sparse sampling via interpolation among samples. However, traditional hyper-reduction techniques do not preserve gradient fields. This implies that hyper-reduced models of Hamiltonian systems are no longer Hamiltonian. As real-world processes tend to be nonlinear, a lack of efficient and physically compatible dimension reduction of general nonlinearities comes to the fore.

To the best of our knowledge, only a few works have considered hyper-reduction methods that preserve Hamiltonian structures. Although these works introduce interesting ideas, they appear rather *ad hoc* or lack a rigorous theoretical analysis of the proposed approximations. In [4] the reduced Hamiltonian is approximated with a Taylor polynomial expansion truncated at the second term. As reported by the authors, the scheme is only effective for asymptotically stable systems and when the expansion is performed around an equilibrium point. These assumptions rule out many important cases and are generally not met by evolution problems stemming from the semi-discretization of partial differential equations. A cubature approach, the Energy-Conserving Sampling and Weighting (ECSW) scheme, is presented in [10]: the nonlinear vector field obtained from the semi-discretization of a Hamiltonian PDE is approximated with a weighted average of the field components on a coarser mesh. The method is, however, limited to finite element discretization of Hamiltonian PDEs, and requires a very expensive offline phase, especially for parametric problems. Finally, the lifting technique introduced in [16] transforms a general nonlinear system into an equivalent problem in polynomial form via a change of coordinates and auxiliary variables. Although non-polynomial nonlinearities are eliminated, the problem in the new coordinate system no longer possesses the geometric structure of the original model. A variation of the discrete empirical interpolation method (DEIM) [2, 7] has been proposed in [6]: the nonlinear Hamiltonian gradient is approximated in the space where the DEIM projection is orthogonal. The Hamiltonian structure is preserved since orthogonal projections preserve gradients, but the method does not guarantee that the resulting approximation is accurate. In a recent preprint [26], DEIM hyper-reduction is applied to a nonlinear vector-valued function G obtained by decomposing the Hamiltonian into the Euclidean product of G with a constant vector. The gradient of the resulting operator provides an approximation of the original Hamiltonian gradient but there is no guarantee on the accuracy of such approximation nor on asymptotic convergence as the DEIM space is enlarged.

We propose a novel gradient-preserving hyper-reduction strategy to construct surrogate models with the following properties: (i) they are Hamiltonian; (ii) they can be solved at a computational cost independent of the size of the full model; (iii) they are provably accurate; and (iv) the preservation of the full order Hamiltonian is ensured asymptotically. The proposed approach targets the *reduced* nonlinear operator, in contrast to traditional hyper-reduction techniques where the nonlinear high-

dimensional function is approximated first and then the resulting approximation is projected onto the reduced space. In particular, we first map the full order nonlinear Hamiltonian gradient into the reduced space via a structure-preserving (here symplectic) projection. Then, the nonlinear part of the reduced Hamiltonian is written as the sum of d terms, where d is typically of the order of the size of the full model. Although the aforementioned decomposition is similar to the one of [26], we do not approximate the resulting d -valued nonlinear function but rather we propose to approximate the Hamiltonian gradient via a suitable DEIM projection of the Jacobian of the nonlinear function. We derive *a priori* error estimates of the error between the full model solution and its hyper-reduced approximation and of the error in the conservation of the Hamiltonian. These results show that the hyper-reduced model is asymptotically as accurate as the reduced model. Since the target accuracy is the one of the reduced model, the hyper-reduction allows to obtain accurate solutions and to ensure exact Hamiltonian conservation with DEIM sizes much smaller than d and, hence, at a significantly reduced computational cost.

Whenever the dynamics of the problem does not allow for small DEIM approximations and, hence, enough computational savings, we let the proposed gradient-preserving hyper-reduction change in time. We derive an adaptive approach that extends to Hamiltonian gradients the adaptive discrete empirical interpolation method (ADEIM) strategy introduced in [21]. The DEIM basis is updated in time with the low-rank factor that minimizes a residual of the nonlinear Jacobian at suitably chosen sampling points. In particular, we extend the method of [21] to updates of general rank and derive an algorithm for the optimal choice of the sampling points. A detailed analysis of the computational complexity of the adaptive hyper-reduction shows that, if the adaptation is implemented in an efficient way, the complexity reduction due to a smaller DEIM basis (compared to the non-adaptive algorithm) outweighs the extra computational cost of constructing the update.

The remainder of the paper is organized as follows. In Section 2 we introduce Hamiltonian dynamical systems and discuss their symplectic model order reduction. Section 3 concerns the structure-preserving DEIM hyper-reduction of the Hamiltonian gradient: we first derive the hyper-reduced model, then discuss how to construct the DEIM projection, and finally establish *a priori* estimates of the error between the full model solution and the hyper-reduced solution and of the error in the conservation of the Hamiltonian. Section 4 is devoted to the adaptive gradient-preserving hyper-reduction method and a summary of the scheme is presented in Algorithm 3. In Section 5 the proposed methods are tested on a set of numerical experiments. Some conclusions and open questions are presented in Section 6.

2 Full order system and its model order reduction

Let $\mathcal{T} := (t_0, T] \subset \mathbb{R}$ be a temporal interval, let $\mathcal{P} \subset \mathbb{R}^p$, with $p \geq 1$, be a compact set of parameters, and let $V_{2n} \subset \mathbb{R}^{2n}$ be a vector space. For each $\eta \in \mathcal{P}$, we consider the Hamiltonian dynamical system: given $y^0(\eta) \in V_{2n}$, find $y(\cdot, \eta) \in C^1(\mathcal{T}; V_{2n})$ such that

$$\begin{cases} \dot{y}(t, \eta) = J_{2n} \nabla_y \mathcal{H}(y(t, \eta), \eta), & t \in \mathcal{T}, \\ y(t_0, \eta) = y^0(\eta), \end{cases} \quad (2.1)$$

where $y : \mathcal{T} \times \mathcal{P} \rightarrow V_{2n}$ is the state variable and the matrix $J_{2n} \in \mathbb{R}^{2n \times 2n}$, the so-called canonical Poisson tensor, is defined as

$$J_{2n} = \begin{pmatrix} 0_n & I_n \\ -I_n & 0_n \end{pmatrix}.$$

The function $\mathcal{H} : V_{2n} \times \mathcal{P} \rightarrow \mathbb{R}$ is the Hamiltonian of the system and we write it in the following general form

$$\mathcal{H}(y, \eta) = \frac{1}{2} y^\top L(\eta) y + y^\top f(\eta) + \mathcal{G}(\eta) + \mathcal{N}(y, \eta), \quad (2.2)$$

where $L(\eta) \in \mathbb{R}^{2n \times 2n}$ is a symmetric positive semi-definite matrix, $f(\eta) \in \mathbb{R}^n$, $\mathcal{G}(\eta) \in \mathbb{R}$ and $\mathcal{N}(\cdot, \eta)$ is a nonlinear function of the state variable. The Hamiltonian is a conserved quantity of system (2.1), namely it remains constant along solution trajectories. Moreover, the phase space of Hamiltonian systems has a symplectic geometric structure. This means that the vector space V_{2n} admits a basis $\{e_i\}_{i=1}^{2n}$ which is symplectic and orthonormal, that is

$$e_i^\top J_{2n} e_j = (J_{2n})_{i,j} \quad \text{and} \quad (e_i, e_j) = \delta_{i,j}, \quad \forall i, j = 1 \dots, 2n,$$

where (\cdot, \cdot) is the Euclidean inner product. We refer to [18, Chapter 10] for a detailed introduction to Hamiltonian systems.

To ensure well-posedness of (2.1) we assume that, for each parameter $\eta \in \mathcal{P}$, the Hamiltonian gradient $\nabla_y \mathcal{H}(\cdot, \eta)$ is Lipschitz continuous in the Euclidean norm uniformly with respect to time.

2.1 Symplectic model order reduction

When the number n of degrees of freedom is large and system (2.1) needs to be solved for many instances of the parameter η , model order reduction can be used to reduce the complexity of the original system and thus to speed up the computationally expensive resulting numerical simulations. Among model order reduction techniques, we consider reduced basis methods (RBM), which construct an approximation space of low dimension, the so-called reduced space, from a collection of simulation data corresponding to full order solutions at sampled values of time and parameters. A low-dimensional model is then obtained via a suitable projection of the full-order dynamics onto the reduced space.

More in details, we approximate the state $y(t, \eta)$, for any $t \in \mathcal{T}$ and $\eta \in \mathcal{P}$, as

$$y_{rb}(t, \eta) = \sum_{i=1}^{2k} z_i(t, \eta) a_i = A z(t, \eta),$$

where $k \ll n$, $A = [a_1 \dots a_{2k}] \in \mathbb{R}^{2n \times 2k}$ is the reduced basis and $z(t, \eta) \in \mathbb{R}^{2k}$ is the vector of expansion coefficients. In order to preserve the Hamiltonian structure of the full model, we require the matrix A to be symplectic, that is, $A^\top J_{2n} A = J_{2k}$, and orthogonal, that is, $A^\top A = I_{2k}$. If A is an orthogonal symplectic matrix, then $A^\top J_{2n} = J_{2k} A^\top$, see e.g. [22, Lemma 3.3]. Projecting the full order model (2.1) onto the space V_{2k} spanned by the columns of A yields the reduced model: for any $\eta \in \mathcal{P}$, find $z(\cdot, \eta) \in C^1(\mathcal{T}; V_{2k})$ such that

$$\begin{cases} \dot{z}(t, \eta) = J_{2k} \nabla_z \mathcal{H}_r(z(t, \eta), \eta), & t \in \mathcal{T}, \\ z(t_0, \eta) = z^0(\eta) := A^\top y^0(\eta), \end{cases} \quad (2.3)$$

where the reduced Hamiltonian is obtained from (2.2) as

$$\mathcal{H}_r(z, \eta) := \mathcal{H}(A z, \eta) = \frac{1}{2} z^\top L_r(\eta) z + z^\top f_r(\eta) + \mathcal{G}(\eta) + \mathcal{N}_r(z, \eta),$$

with $L_r(\eta) := A^\top L(\eta) A$, $f_r(\eta) := A^\top f(\eta) \in \mathbb{R}^{2k}$ and $\mathcal{N}_r := \mathcal{N} \circ A$.

An orthogonal and symplectic reduced basis can be constructed from a set of full model solutions using SVD-type strategies, such as cotangent lift, complex SVD, or nonlinear programming [22], or with the symplectic greedy algorithm of [1].

3 Hyper-reduction of the Hamiltonian gradient

Assuming the affine separability of the operators $L(\eta)$ and $f(\eta)$ in (2.2), the major computational cost in solving the reduced model (2.3) comes from the nonlinear term \mathcal{N}_r of the Hamiltonian. If standard hyper-reduction techniques are applied to the reduced Hamiltonian gradient $\nabla_z \mathcal{H}_r$, the

resulting approximate function is generally no longer a gradient field. To address this shortcoming we pursue a different approach. First, we consider a decomposition of the nonlinear part of the reduced Hamiltonian similar to [26], that is

$$\mathcal{N}_r(z, \eta) = \sum_{i=1}^d v_i h_i(Az, \eta) = v^\top h(Az, \eta), \quad \text{for all } z \in V_{2k}, \eta \in \mathcal{P}, \quad (3.1)$$

where d is some natural number, $v \in \mathbb{R}^d$ is a constant vector and $h : V_{2n} \times \mathcal{P} \rightarrow \mathbb{R}^d$. A decomposition of the Hamiltonian of the form (3.1) can be derived in many cases of interest. For example, the Hamiltonian given by the energy of a system of particles can be written as the sum of the contribution of each particle; or, if (2.1) results from the semi-discretization of a PDE via a local approximation, e.g. a finite element or finite volume scheme, one may think of h_i as the contribution of the i th mesh element to the total Hamiltonian. We refer to [18] and [13, Chapter I] for several examples of Hamiltonian in this form.

Using the decomposition (3.1), the gradient of the nonlinear part of the reduced Hamiltonian reads

$$\nabla_z \mathcal{N}_r(z, \eta) = A^\top J_{\eta, h}^\top(Az)v, \quad \text{for all } z \in V_{2k}, \eta \in \mathcal{P}, \quad (3.2)$$

where $J_{\eta, h} \in \mathbb{R}^{d \times 2n}$ is the Jacobian of $h(\cdot, \eta)$. The idea is then to use discrete empirical interpolation to approximate the term $J_{\eta, h}(Az)A \in \mathbb{R}^{d \times 2k}$, namely the Jacobian mapped to the reduced space. The projected reduced Jacobian is

$$\mathbb{P} J_{\eta, h}(Az)A, \quad \text{where } \mathbb{P} := U(P^\top U)^{-1}P^\top \in \mathbb{R}^{d \times d}. \quad (3.3)$$

Here, $U \in \mathbb{R}^{d \times m}$ is the so-called DEIM basis with $m \ll d$, and $P := [\mathbf{e}_{\beta(1)}, \dots, \mathbf{e}_{\beta(m)}] \in \mathbb{R}^{d \times m}$, where \mathbf{e}_i is the i th unit vector of \mathbb{R}^d and $\{\beta(1), \dots, \beta(m)\} \subset \{1, \dots, d\}$ are interpolation indices. The DEIM projection introduced in (3.3) can be equivalently seen as an approximation of the nonlinear term \mathcal{N}_r in (3.1) by

$$\mathcal{N}_{hr}(z, \eta) := v^\top \mathbb{P} h(Az, \eta) \quad \text{for all } z \in V_{2k}, \eta \in \mathcal{P}. \quad (3.4)$$

This allows to show that the dynamical system resulting from the hyper-reduction is still Hamiltonian with the nonlinear term of the Hamiltonian approximated as in (3.4). The hyper-reduced model reads: for any $\eta \in \mathcal{P}$, find $z(\cdot, \eta) \in C^1(\mathcal{T}; V_{2k})$ such that

$$\begin{cases} \dot{z}(t, \eta) = J_{2k} \nabla_z \mathcal{H}_{hr}(z(t, \eta), \eta), & t \in \mathcal{T}, \\ z(t_0, \eta) = z^0(\eta) := A^\top y^0(\eta), \end{cases} \quad (3.5)$$

where the hyper-reduced Hamiltonian is

$$\mathcal{H}_{hr}(z, \eta) = \frac{1}{2} z^\top L_r(\eta) z + z^\top f_r(\eta) + \mathcal{G}(\eta) + \mathcal{N}_{hr}(z, \eta), \quad \text{for all } z \in V_{2k}, \eta \in \mathcal{P},$$

and its gradient reads $\nabla_z \mathcal{H}_{hr}(z, \eta) = L_r(\eta)z + f_r(\eta) + A^\top J_{\eta, h}^\top(Az)\mathbb{P}^\top v$, for all $z \in V_{2k}$ and $\eta \in \mathcal{P}$.

Remark 3.1. A key role in this approach is played by the decomposition (3.1), which is not unique, and thus by the choice of d . Indeed, let us assume that, for fixed $z \in V_{2k}$ and $\eta \in \mathcal{P}$, each entry of $h(y, \eta)$, with $y := Az$, depends on s_1 components among the first n entries of y and on s_2 components among the last n entries of y , with $s_1, s_2 \leq n$. In this case, every row of $J_{\eta, h}$ has at most $s_1 + s_2$ non-zero elements. Then the evaluation of the gradient (3.2) of the reduced Hamiltonian has computationally complexity $O((s_1 + s_2)dk)$, while the cost of computing the gradient of the hyper-reduced Hamiltonian (3.4) is of order $O((s_1 + s_2)mk)$. Based on this observation one might be tempted to choose a decomposition (3.1) with a small d and bypass the hyper-reduction entirely. This choice is however often associated with large values of s_1 and s_2 since typically $(s_1 + s_2)d$ is, at least, of the order of n . The choice of the decomposition should instead be driven as to maximize the sparsity of the Jacobian matrix $J_{\eta, h} \in \mathbb{R}^{d \times 2n}$, hence maximizing the efficacy of the hyper-reduction. We refer to the numerical experiments in Section 5 for concrete examples of such decomposition.

3.1 Construction of the DEIM projection

Based on the observation that \mathcal{N}_r is approximated by \mathcal{N}_{hr} as in (3.4), the algorithm proposed in [26] seeks to approximate the factor h of the decomposition (3.1). However, this does not lead to any guarantee on the accuracy of the approximation of the reduced Hamiltonian gradient and hence on the quality of the hyper-reduced model (3.5). What we propose instead is to minimize the DEIM projection error of the reduced Jacobian, $J_{\eta,h}(A \cdot)A \in \mathbb{R}^{d \times 2k}$, once the reduced basis A has been constructed.

To build the DEIM projection, we compute snapshots in the reduced space V_{2k} as $\{A^\top y^{\ell_i}(\eta_j)\}_{i,j}$ for $j = 1, \dots, N_p$ and $i = 1, \dots, N_s$, where $y^{\ell_i}(\eta_j)$ is the full model solution at time t^{ℓ_i} and parameter η_j . We collect the corresponding snapshots of the reduced Jacobian in the matrix

$$M_J = [J_{\eta_1,h}(AA^\top y^{\ell_1}(\eta_1))A \dots J_{\eta_{N_p},h}(AA^\top y^{\ell_{N_s}}(\eta_{N_p}))A] \in \mathbb{R}^{d \times 2kN_sN_p}. \quad (3.6)$$

The DEIM basis $U \in \mathbb{R}^{d \times m}$ in (3.3) is obtained from M_J via proper orthogonal decomposition (POD). Observe that the snapshot matrix M_J can potentially have a large number of columns: to curb the high computational cost to derive the DEIM basis from M_J , one could make use of fast algorithms, such as randomized SVD [14].

Once the DEIM basis is fixed, there are several ways to select the DEIM interpolation indices in such a way that $P^\top U$ is non-singular. In this work we focus on the greedy algorithm of [7, Algorithm 1]. An alternative choice is, for example, the QDEIM algorithm introduced in [9], which is based on a QR factorization with column pivoting of the matrix U .

Remark 3.2. In principle, one may approximate the full Jacobian $J_{\eta,h}$ rather than the reduced Jacobian $J_{\eta,h}(AA^\top \cdot)A$. However, there are (at least) two major issues in dealing with the full Jacobian. First, the snapshot matrix M_J has $2nN_sN_p$ columns instead of $2kN_sN_p$, where $n \gg k$. In many applications, already for one-dimensional problems, this matrix is too large to be stored, and the cost of computing its singular values and vectors is prohibitive. This is particularly relevant in the adaptive approach, see Section 4, when the DEIM projection is updated online. Second, the full Jacobian $J_{\eta,h}$ usually exhibits diagonal (or sparsity) patterns so that the associated snapshot matrix has full or almost full rank. This implies that one has to select $m \approx d$ DEIM basis functions to achieve a sufficiently accurate approximation, making hyper-reduction basically ineffective. On the contrary, if the reduced Jacobian is considered, it is found in practice that the singular values of M_J exhibit a much faster decay, which allows for an efficient hyper-reduction. We refer to Figure 8 in Section 5.2 for a numerical example that shows this behavior.

3.2 A priori convergence estimates

In this section we derive an estimate on the error between the full and hyper-reduced solution. First we show that the error of the approximation of the reduced Jacobian given by the DEIM projection is bounded analogously to [7, Lemma 3.2], namely by a quantity that depends on the neglected singular values of the snapshot matrix M_J in (3.6) and on $(P^\top U)^{-1}$.

Lemma 3.3. *Let $M_J \in \mathbb{R}^{d \times 2kN_sN_p}$ be the snapshot matrix of the reduced Jacobian defined in (3.6). Assume that M_J has rank r_M . Let $\mathbb{P} = U(P^\top U)^{-1}P^\top$ be the DEIM projection defined in (3.3) and derived as in Section 3.1. Then,*

$$\|(I - \mathbb{P})J_{\eta_j,h}(AA^\top y^{s_i}(\eta_j))A\|_2 \leq \kappa \sqrt{\sum_{\ell=m+1}^{r_M} \sigma_\ell^2} \quad \forall i = 1, \dots, N_s, j = 1, \dots, N_p,$$

where $\{\sigma_\ell\}_{\ell=1}^{r_M}$ are the singular values of M_J and $\kappa := \|(P^\top U)^{-1}\|_2$.

Proof. Let us introduce $M^\ell := J_{\eta_j, h}(AA^\top y^{s_i}(\eta_j))A$, for $\ell = N_s(j-1) + i$, with $i = 1, \dots, N_s$ and $j = 1, \dots, N_p$. A straightforward extension of [7, Lemma 3.2] allows to bound the Frobenius norm of the DEIM projection error in the reduced Jacobian as,

$$\|(I - \mathbb{P})M^\ell\|_F \leq \|(P^\top U)^{-1}\|_2 \|(I - UU^\top)M^\ell\|_F \leq \kappa \|(I - UU^\top)M_J\|_F.$$

The conclusion follows by applying the standard result of best low-rank approximation to M_J , see e.g. [23, Proposition 6.1]. \square

The error between the full order and hyper-reduced solution can be bounded by the error between the full order solution and its projection onto the reduced space and the DEIM projection error of the reduced Jacobian. The following theorem extends to our setting the result in [8, Theorem 3.1].

Theorem 3.4. *For any given $\eta \in \mathcal{P}$, let $y(\cdot, \eta) \in C^1(\mathcal{T}, V_{2n})$ be the solution of the full model (2.1) and let $z(\cdot, \eta) \in C^1(\mathcal{T}, V_{2k})$ be the solution of the hyper-reduced system (3.5). Let \mathbb{P} be the DEIM projection defined in (3.3). Assume that, for every $\eta \in \mathcal{P}$, the Jacobian $J_{\eta, h}$ of h (3.1) is Lipschitz continuous in the norm $\|\cdot\|$ with constant $\mathcal{L}_h(\eta)$. Then,*

$$\begin{aligned} \|y - Az\|_{L^2(\mathcal{T} \times \mathcal{P}; V_{2n})}^2 &\leq C_1(T) \|y - AA^\top y\|_{L^2(\mathcal{T} \times \mathcal{P}; V_{2n})}^2 \\ &\quad + C_2(T) \|(I - \mathbb{P})J_{\eta, h}(AA^\top y)A\|_{L^2(\mathcal{T} \times \mathcal{P}; V_{2n})}^2, \end{aligned} \quad (3.7)$$

where $C_1(T) := \Delta\mathcal{T} \max_{\eta \in \mathcal{P}} (C_\eta(T)\alpha^2(\eta)) + 1$ and $C_2(T) := \Delta\mathcal{T} \|v\|^2 \max_{\eta \in \mathcal{P}} C_\eta(T)$, with

$$C_\eta(T) := \begin{cases} \beta^{-1}(\eta)(e^{2\beta(\eta)(T-t_0)} - 1), & \text{if } \beta(\eta) \neq 0, \\ 2(T-t_0), & \text{if } \beta(\eta) = 0, \end{cases}$$

$\alpha(\eta) := \|A^\top K(\eta)\|_2 + \mathcal{L}_N(\eta)$, with $\mathcal{L}_N(\eta)$ Lipschitz continuity constant of $\nabla\mathcal{N}(\cdot, \eta)$, $\beta(\eta) := \mu(K(\eta)) + \mathcal{L}_h(\eta) \|(P^\top U)^{-1}\|_2 \|v\|$, and $\mu(K(\eta))$ is the logarithmic norm of $K(\eta) := J_{2n}L(\eta)$ with respect to the 2-norm.

Proof. Let us fix the parameter $\eta \in \mathcal{P}$. The error at each time $t \in \mathcal{T}$ can be split as

$$e(t, \eta) := y(t, \eta) - Az(t, \eta) = e_p(t, \eta) + e_h(t, \eta),$$

where $e_p(t, \eta) := y(t, \eta) - AA^\top y(t, \eta)$ is the projection error and $e_h(t, \eta) := AA^\top y(t, \eta) - Az(t, \eta)$. Differentiating e_h with respect to time, using (2.1) and (3.5), and the symplecticity of A results in

$$\dot{e}_h(t, \eta) = AA^\top \dot{y}(t, \eta) - A\dot{z}(t, \eta) = AA^\top K(\eta)e_h(t, \eta) + s(t, \eta),$$

where $s(t, \eta) := AA^\top K(\eta)e_p(t, \eta) + AJ_{2k}(A^\top \nabla_y \mathcal{N}(y, \eta) - \nabla_z \mathcal{N}_{hr}(z, \eta))$ and $K(\eta) := J_{2n}L(\eta)$. The norm of s can be bounded as

$$\|s(t, \eta)\| \leq \|A^\top K(\eta)\|_2 \|e_p(t, \eta)\| + \|A^\top \nabla_y \mathcal{N}(y, \eta) - \nabla_z \mathcal{N}_{hr}(z, \eta)\|. \quad (3.8)$$

The second term in (3.8) can be split as follows,

$$\begin{aligned} \|A^\top \nabla_y \mathcal{N}(y, \eta) - \nabla_z \mathcal{N}_{hr}(z, \eta)\| &\leq \|A^\top \nabla_y \mathcal{N}(y, \eta) - A^\top \nabla_y \mathcal{N}(AA^\top y, \eta)\| \\ &\quad + \|A^\top \nabla_y \mathcal{N}(AA^\top y, \eta) - \nabla_z \mathcal{N}_{hr}(A^\top y, \eta)\| \\ &\quad + \|\nabla_z \mathcal{N}_{hr}(A^\top y, \eta) - \nabla_z \mathcal{N}_{hr}(z, \eta)\|. \end{aligned} \quad (3.9)$$

We consider the three terms on the right-hand side separately. First observe that, if $\nabla_y \mathcal{H}(\cdot, \eta)$ is Lipschitz continuous in the $\|\cdot\|$ -norm with constant $\mathcal{L}_H(\eta)$, then $\nabla\mathcal{N}(\cdot, \eta)$ is also Lipschitz continuous with constant $\mathcal{L}_N(\eta) \leq \mathcal{L}_H(\eta) + \|L(\eta)\|_2$. This implies that

$$\|A^\top \nabla_y \mathcal{N}(y, \eta) - A^\top \nabla_y \mathcal{N}(AA^\top y, \eta)\| \leq L_N(\eta) \|e_p(t, \eta)\|.$$

Moreover, using the decomposition of the Hamiltonian in (3.1) results in

$$\begin{aligned} \|A^\top \nabla_y \mathcal{N}(AA^\top y, \eta) - \nabla_z \mathcal{N}_{hr}(A^\top y, \eta)\| &= \|A^\top J_{\eta,h}^\top(AB^\top y)v - A^\top J_{\eta,h}^\top(AB^\top y)\mathbb{P}^\top v\| \\ &\leq \|v\| \|(I - \mathbb{P})J_{\eta,h}(AB^\top y)A\|_2, \end{aligned}$$

and similarly

$$\begin{aligned} \|\nabla_z \mathcal{N}_{hr}(A^\top y, \eta) - \nabla_z \mathcal{N}_{hr}(z, \eta)\| &= \|A^\top J_{\eta,h}^\top(AB^\top y)\mathbb{P}^\top v - A^\top J_{\eta,h}^\top(Az)\mathbb{P}^\top v\| \\ &\leq L_h(\eta) \|AB^\top y - Az\| \|\mathbb{P}^\top v\| \leq \gamma(\eta) \|e_h(t, \eta)\|, \end{aligned} \quad (3.10)$$

where $\gamma(\eta) := L_h(\eta) \|(P^\top U)^{-1}\|_2 \|v\|$. We can now plug these three bounds into (3.9) and (3.8) to obtain

$$\|s(t, \eta)\| \leq \alpha(\eta) \|e_p(t, \eta)\| + \gamma(\eta) \|e_h(t, \eta)\| + \|v\| \|W(t, \eta)\|_2, \quad (3.11)$$

where $\alpha(\eta) := \|A^\top K(\eta)\|_2 + L_N(\eta)$, and $W(t, \eta) := (I - \mathbb{P})J_{\eta,h}(AB^\top y(t, \eta))A$.

The time derivative of the error norm gives

$$\frac{d}{dt} \|e_h(t, \eta)\| = \frac{1}{\|e_h(t, \eta)\|} (AA^\top K(\eta)e_h(t, \eta), e_h(t, \eta)) + \frac{1}{\|e_h(t, \eta)\|} (s(t, \eta), e_h(t, \eta)). \quad (3.12)$$

The first term on the right-hand side of (3.12) can be bounded as in [8, Theorem 3.1], namely

$$\frac{1}{\|e_h(t, \eta)\|} (AA^\top K(\eta)e_h(t, \eta), e_h(t, \eta)) \leq \mu(K(\eta)) \|e_h(t, \eta)\|, \quad (3.13)$$

using the fact that $(AA^\top K(\eta)e_h, e_h) = (AA^\top K(\eta)A\tilde{e}_h, A\tilde{e}_h) \leq \mu(A^\top KA) \|\tilde{e}_h\|^2$, with $\tilde{e}_h := A^\top y - z$.

The second term on the right-hand side of (3.12) can be bounded using (3.11),

$$\frac{1}{\|e_h(t, \eta)\|} (s(t, \eta), e_h(t, \eta)) \leq \alpha(\eta) \|e_p(t, \eta)\| + \gamma(\eta) \|e_h(t, \eta)\| + \|v\| \|W(t, \eta)\|_2. \quad (3.14)$$

Plugging (3.13) and (3.14) into (3.12) we have

$$\frac{d}{dt} \|e_h(t, \eta)\| \leq \beta(\eta) \|e_h(t, \eta)\| + b(t, \eta), \quad (3.15)$$

where $\beta(\eta) := \mu(K(\eta)) + \gamma(\eta)$, and $b(t, \eta) := \alpha(\eta) \|e_p(t, \eta)\| + \|v\| \|W(t, \eta)\|_2$.

Starting from (3.15), we apply the Gronwall inequality [12], to get

$$\|e_h(t, \eta)\|^2 \leq C_\eta(t) \int_{t_0}^t (\alpha^2(\eta) \|e_p(s, \eta)\|^2 + \|v\|^2 \|W(s, \eta)\|_2^2) ds,$$

where $C_\eta(t) := 2 \int_{t_0}^t e^{2\beta(\eta)(t-s)} ds$. This implies that the error is bounded as

$$\begin{aligned} \|e\|_{L^2(\mathcal{T} \times \mathcal{P}; V_{2n})}^2 &\leq \|e_p\|_{L^2(\mathcal{T} \times \mathcal{P}; V_{2n})}^2 + \Delta \mathcal{T} \int_{\mathcal{P}} C_\eta(T) \int_{t_0}^T (\alpha^2(\eta) \|e_p(s, \eta)\|^2 + \|v\|^2 \|W(s, \eta)\|_2^2) dt d\eta \\ &\leq \int_{\mathcal{P}} (\Delta \mathcal{T} C_\eta(T) \alpha^2(\eta) + 1) \|y(\cdot, \eta) - AA^\top y(\cdot, \eta)\|_{L^2(\mathcal{T}; V_{2n})}^2 d\eta \\ &\quad + \Delta \mathcal{T} \|v\|^2 \int_{\mathcal{P}} C_\eta(T) \|(I - \mathbb{P})J_{\eta,h}(AB^\top y(\cdot, \eta))A\|_{L^2(\mathcal{T}; V_{2n})}^2 d\eta, \end{aligned}$$

which yields the conclusion. \square

The first term on the right-hand side of (3.7) is controlled via the reduced space, while the second term can be minimized via a suitable construction of the DEIM basis and according to Lemma 3.3.

The dependence of the constants in the bound (3.7) on the norm of the vector v can be avoided by a suitable normalization of the decomposition (3.1).

For Jacobian matrices having a particular structure, the Lipschitz continuity assumption of $J_{\eta,h}$ in Theorem 3.4 might not be needed. An example often encountered in applications is when the i th entry of $h(y, \eta)$ only depends on the i th pair of symplectic variables, namely on the i th and $(i+n)$ th components of y , for any $y \in V_{2n}$. In this case, $d = n$ and $J_{\eta,h} \in \mathbb{R}^{n \times 2n}$ is formed of two $n \times n$ diagonal blocks. This implies that $\nabla_z \mathcal{N}_{hr} = J_{\eta,h}^\top \mathbb{P}^\top v$ is of the form $D \nabla \mathcal{N}$ where

$$D := \text{diag}((\mathbb{P}^\top v)_1, \dots, (\mathbb{P}^\top v)_n, (\mathbb{P}^\top v)_1, \dots, (\mathbb{P}^\top v)_n) \in \mathbb{R}^{2n \times 2n}.$$

Therefore, the bound in (3.10) becomes

$$\begin{aligned} \|\nabla_z \mathcal{N}_{hr}(A^\top y, \eta) - \nabla_z \mathcal{N}_{hr}(z, \eta)\| &= \|A^\top D(\nabla_y \mathcal{N}(AA^\top y, \eta) - \nabla_y \mathcal{N}(Az, \eta))\| \\ &\leq \|D\|_2 \mathcal{L}_{\mathcal{N}}(\eta) \|AA^\top y - Az\|, \end{aligned}$$

where $\|D\|_2 = \sigma_{\max}(D) \leq \|\mathbb{P}^\top v\|_2 \leq \|(P^\top U)^{-1}\|_2 \|v\|$. Therefore, (3.10) holds with $\gamma(\eta) := \mathcal{L}_{\mathcal{N}}(\eta) \|(P^\top U)^{-1}\|_2 \|v\|$ and no Lipschitz continuity assumption on $J_{\eta,h}$ is required.

3.3 Conservation of the Hamiltonian

The Hamiltonian is a conserved quantity of the system. In this section we assess the error that we introduce in the conservation of the Hamiltonian by approximating it via hyper-reduction. In the following result we show that the error between the Hamiltonian evaluated at the full model solution and at the hyper-reduced solution is bounded by the approximation error of \mathcal{N} . This implies that the hyper-reduced model guarantees preservation of the Hamiltonian for sufficiently large DEIM bases, that is, when the accuracy of the hyper-reduced model reaches the accuracy of the reduced model and up to errors due to the time integration scheme. We refer to Section 5 for several numerical tests that corroborate this result.

Proposition 3.5. *Let $\eta \in \mathcal{P}$ be fixed. Let $y^j(\eta)$ be an approximation of the solution $y(t^j, \eta)$ of the full order system (2.1) at time t^j , with $j = 1, \dots, N_t$, obtained with a user-defined numerical time integrator. Similarly, let $z^j(\eta)$ be an approximation of the solution $z(t^j, \eta)$ of the hyper-reduced system (3.5) at time t^j . Assume that $y^0(\eta) \in \text{Col}(A)$ and $h(AA^\top y^0(\eta), \eta) \in \text{Col}(U)$, where Col denotes the column space. Then, the error $\Delta \mathcal{H}_j(\eta) := |\mathcal{H}(y^j(\eta), \eta) - \mathcal{H}(Az^j(\eta), \eta)|$ satisfies*

$$\Delta \mathcal{H}_j(\eta) \leq |v^\top (I - \mathbb{P}) h(Az^j(\eta), \eta)| + \varepsilon_{\mathcal{H}}^{[t^0, t^j]} + \varepsilon_{\mathcal{H}_{hr}}^{[t^0, t^j]},$$

where $\varepsilon_{\mathcal{H}}^{[t^0, t^j]} := |\mathcal{H}(y^j) - \mathcal{H}(y^0)|$ and $\varepsilon_{\mathcal{H}_{hr}}^{[t^0, t^j]} := |\mathcal{H}_{hr}(z^j) - \mathcal{H}_{hr}(z^0)|$ are the errors in the Hamiltonian conservation, in the temporal interval $[t^0, t^j]$, associated with the chosen temporal integrator.

Proof. In this proof we omit the dependence of y^j , z^j and \mathcal{H} on η . The Hamiltonian error at the generic time instant t^j can be bounded as

$$\begin{aligned} \Delta \mathcal{H}_j &\leq |\mathcal{H}(y^j) - \mathcal{H}(y^0)| + |\mathcal{H}_{hr}(z^j) - \mathcal{H}_{hr}(z^0)| \\ &\quad + |\mathcal{H}(Az^0) - \mathcal{H}_{hr}(z^0)| + |\mathcal{H}(Az^j) - \mathcal{H}_{hr}(z^j)| + \Delta \mathcal{H}_0(\eta). \end{aligned} \tag{3.16}$$

The first two terms in (3.16) are $\varepsilon_{\mathcal{H}}^{[t^0, t^j]}$ and $\varepsilon_{\mathcal{H}_{hr}}^{[t^0, t^j]}$, respectively, and measure the Hamiltonian conservation with respect to the initial value in the full and hyper-reduced systems. These quantities only depend on the time integration scheme.

The term $|\mathcal{H}(Az^0) - \mathcal{H}_{hr}(z^0)| = |v^\top (I - \mathbb{P}) h(Az^0)|$ vanishes since $h(Az^0) \in \text{Col}(U)$ by assumption. Similarly, the term $\Delta \mathcal{H}_0(\eta)$ vanishes due to the injectivity of the linear map A and the assumption $y^0 \in \text{Col}(A)$.

The conclusion follows by the definition of the full order and reduced Hamiltonian. \square

This result hinges on the assumptions that $y^0(\eta) \in \text{Col}(A)$ and $h(AA^\top y^0, \eta) \in \text{Col}(U)$ for any value of the parameter $\eta \in \mathcal{P}$. These conditions can be enforced via a shifting of the state variable and of the operator h . Let us introduce the variable $y_s(t, \eta) := y(t, \eta) - y^0(\eta)$ and the shifted operator $h_s(y(t, \eta), \eta) := h(y(t, \eta), \eta) - h(y^0(\eta), \eta)$, for any $t \in \mathcal{T}$ and $\eta \in \mathcal{P}$. Substituting into the expression of the Hamiltonian (2.2) gives

$$\mathcal{H}_s(y_s, \eta) := \mathcal{H}(y_s + y^0, \eta) = \frac{1}{2} y_s^\top L(\eta) y_s + y_s^\top f_s(\eta) + \mathcal{G}_s(\eta) + v^\top h_s(y_s + y^0, \eta),$$

where $f_s(\eta) := f(\eta) + L(\eta)y^0$ and $\mathcal{G}_s(\eta) = \mathcal{G}(\eta) + 1/2(y^0)^\top L(\eta)y^0 + (y^0)^\top f(\eta) + v^\top h(y^0, \eta)$. Then, the shifted full order system reads

$$\begin{cases} \dot{y}_s = J_{2n} \nabla_{y_s} \mathcal{H}_s(y_s, \eta), & t \in \mathcal{T}, \\ y_s(t_0, \eta) = 0. \end{cases} \quad (3.17)$$

Since $y_s^0 = 0$ trivially belongs to the vector space spanned by the reduced basis A and $h_s(AA^\top y_s^0 + y^0, \eta) = h_s(y^0, \eta) = h(y^0, \eta) - h(y^0, \eta) = 0$ belongs to the space spanned by the DEIM basis U , the shifted system (3.17) satisfies the hypotheses of Proposition 3.5. The shifted system (3.17) is the one we consider as full order model in all numerical tests of Section 5.

4 Adaptive gradient-preserving hyper-reduction

The DEIM approximation of the reduced Jacobian described in Section 3 is built in the offline phase and does not change during the time integration of the hyper-reduced system. However, in many cases of interest, such as convection-dominated phenomena and conservative dynamics, it is known that the solution space, under variation of time and parameter, has poor global reducibility properties. An analogous property is observed when considering the space of Hamiltonian gradients, although a rigorous connection between the reducibility of the two spaces is not known. We refer to Section 5.2 for numerical evidence of these considerations.

An effective strategy to address the lack of global reducibility properties, is to let the DEIM projection change in time according to the evolution of the reduced Jacobian. In this section, we derive an adaptive strategy for the hyper-reduction of (2.1) where the DEIM basis is updated in time while preserving the gradient structure of the Hamiltonian vector field. The proposed approach is inspired by the method proposed in [21] and [20] and called ADEIM.

Starting from a DEIM basis $U_0 \in \mathbb{R}^{d \times m}$ and interpolation matrix $P_0 \in \mathbb{R}^{d \times m}$, the idea of the adaptive hyper-reduction is to perform a rank- r update of the DEIM basis to adapt the DEIM pair (U_j, P_j) to (U_{j+1}, P_{j+1}) for $j = 0, \dots, N_a - 1$, where N_a is the number of adaptations. For the sake of exposition, we assume that basis and interpolation points are adapted every δ time instants starting from t^{δ_0} , where $\delta, \delta_0 > 1$ are fixed hyper-parameters. Assuming, for simplicity, that $N_t - \delta_0$ is a multiple of δ , the number of adaptations is $N_a = \delta^{-1}(N_t - \delta_0)$ so that the adaptations are performed at time instants $\{t^{\ell_j}\}_{j=1}^{N_a}$, where $\ell_j := \delta_0 + (j-1)\delta$. We define $\ell_0 := 0$ and note that $t^{\ell_{N_a+1}} = t^{N_t} = T$. In principle, N_a does not need to be fixed *a priori* and it may be determined during time evolution of the hyper-reduced system based on e.g. suitable error criteria.

Between two updates the local hyper-reduced system to be solved in the temporal interval $[t^{\ell_j}, t^{\ell_{j+1}}]$ reads

$$\begin{cases} \dot{z}(t, \eta) = J_{2k} \nabla_z \mathcal{H}_{hr}^j(z(t, \eta), \eta), & t \in (t^{\ell_j}, t^{\ell_{j+1}}], \\ z(t^{\ell_j}, \eta) = z^{\ell_j}(\eta), \end{cases} \quad (4.1)$$

for $j = 0, \dots, N_a$, where the local hyper-reduced Hamiltonian is given by

$$\mathcal{H}_{hr}^j(z, \eta) := \frac{1}{2} z^\top L_r(\eta) z + z^\top f_r(\eta) + \mathcal{G}(\eta) + v^\top \mathbb{P}_j h(Az, \eta),$$

and $\mathbb{P}_j := U_j(P_j^\top U_j)^{-1}P_j^\top$.

In the proposed adaptive hyper-reduction algorithm, the basis update is performed for each instance of the test parameter. Let us then fix the problem parameter $\eta \in \mathcal{P}$. The initial DEIM basis U_0 is constructed in the offline phase from snapshots of the full model solutions in the first δ_0 time steps, namely

$$M_J = [J_{\eta,h}(AA^\top y^1(\eta))A \dots J_{\eta,h}(AA^\top y^{\delta_0}(\eta))A] \in \mathbb{R}^{d \times 2k\delta_0}.$$

The computational cost of computing U_0 from M_J is of the order $O(d^2\delta_0k)$, instead of $O(d^2N_sk)$ as in the non-adaptive case. Observe that one might also construct the initial DEIM pair (U_0, P_0) based on a set of training parameters.

Next, at time instant $t^{\ell_{j+1}}$, with $j = 0, \dots, N_a - 1$, the DEIM pair (U_j, P_j) is updated based on the snapshots of the nonlinear Hamiltonian in a past temporal window of size $w \in \mathbb{N}$, with $w < \delta_0$. More in details, consider the snapshot matrix of the reduced Jacobian in the temporal window $[t^{\ell_{j+1}-w+1}, t^{\ell_{j+1}}]$, namely let

$$F_j := [J_{\eta,h}(Az^{\ell_{j+1}-w+1})A \dots J_{\eta,h}(Az^{\ell_{j+1}})A] \in \mathbb{R}^{d \times \bar{w}},$$

where $\bar{w} := 2kw$. The residual of the DEIM approximation of the columns of F_j is given by $R_j = U_j C_j - F_j \in \mathbb{R}^{d \times \bar{w}}$, where $C_j \in \mathbb{R}^{m \times \bar{w}}$ is the DEIM coefficient matrix $C_j := (P_j^\top U_j)^{-1}P_j^\top F_j$. The adaptive DEIM approach proposed in [21] consists in updating the DEIM basis matrix U_j to U_{j+1} via a rank- r correction, that is

$$U_{j+1} = U_j + \boldsymbol{\alpha}_j \boldsymbol{\beta}_j^\top \quad (4.2)$$

with $\boldsymbol{\alpha}_j \in \mathbb{R}^{d \times r}$ and $\boldsymbol{\beta}_j \in \mathbb{R}^{m \times r}$ of rank $r \in \mathbb{N}$, $r \leq m$. The ADEIM update $\boldsymbol{\alpha}_j \boldsymbol{\beta}_j^\top$ is defined as the rank- r matrix that minimizes the Frobenius norm of the residual at the sampling points collected in the matrix $S_j = [\mathbf{e}_{s_1^{(j)}} \dots \mathbf{e}_{s_{m_s}^{(j)}}] \in \mathbb{R}^{d \times m_s}$ where $s_1^{(j)}, \dots, s_{m_s}^{(j)} \in \{1, \dots, d\}$, namely it minimizes

$$\|S_j^\top (U_{j+1} C_j - F_j)\|_F^2 = \|S_j^\top R_j + S_j^\top \boldsymbol{\alpha}_j \boldsymbol{\beta}_j^\top C_j\|_F^2.$$

With the change of variables $\mathbf{a}_j := S_j^\top \boldsymbol{\alpha}_j \in \mathbb{R}^{m_s \times r}$, and $\mathbf{b}_j := \boldsymbol{\beta}_j \in \mathbb{R}^{m \times r}$, the update (4.2) boils down to solving the minimization problem

$$(\mathbf{a}_j, \mathbf{b}_j) = \arg \min_{(\mathbf{a}, \mathbf{b}) \in \mathcal{V}_r(m_s, m)} \|S_j^\top R_j + \mathbf{a} \mathbf{b}^\top C_j\|_F^2, \quad (4.3)$$

over the space of rank- r matrices defined as

$$\mathcal{V}_r(m_s, m) := \{(\mathbf{a}, \mathbf{b}) \in \mathbb{R}^{m_s \times r} \times \mathbb{R}^{m \times r} : \text{rank}(\mathbf{a}) = \text{rank}(\mathbf{b}) = r\}. \quad (4.4)$$

The number m_s of sampling points is taken such that $m_s \geq m$ and $m_s \ll d$. The first requirement ensures that the minimization problem (4.3) has a non-trivial solution, while the second condition is enforced to avoid working in the potentially high dimension d . Notice that, since only m_s of the d rows of $S_j \mathbf{a}_j \in \mathbb{R}^{d \times r}$ are non-zero, the update (4.2) only modifies m_s rows of the DEIM basis U_j , that is

$$\check{S}_j^\top U_{j+1} = \check{S}_j^\top U_j, \quad (4.5)$$

where $\check{S}_j := [\mathbf{e}_{s_{m_s+1}^{(j)}} \dots \mathbf{e}_{s_d^{(j)}}] \in \mathbb{R}^{d \times (d-m_s)}$, and $\{s_{m_s+1}^{(j)}, \dots, s_d^{(j)}\} := \{1, \dots, d\} \setminus \{s_1^{(j)}, \dots, s_{m_s}^{(j)}\}$.

4.1 Rank- r update of the DEIM basis

The minimization problem (4.3) has been already considered in [21, Lemma 3.5] for rank-1 updates of the DEIM basis. We extend the result to the general case of rank $r > 1$.

Theorem 4.1. Let $r \leq m$ and assume that $C_j \in \mathbb{R}^{m \times \bar{w}}$ has full row-rank m . Let $\mathcal{V}_r(m_s, m)$ be defined as in (4.4). Then, the solution of the minimization problem

$$\min_{(\mathbf{a}, \mathbf{b}) \in \mathcal{V}_r(m_s, m)} \|S_j^\top R_j + \mathbf{a}\mathbf{b}^\top C_j\|_F^2, \quad (4.6)$$

is given by $\mathbf{a} = [a_1 \dots a_r] \in \mathbb{R}^{m_s \times r}$ and $\mathbf{b} = [b_1 \dots b_r] \in \mathbb{R}^{m \times r}$ where b_1, \dots, b_r are the eigenvectors of the generalized eigenvalue problem

$$C_j(S_j^\top R_j)^\top (S_j^\top R_j) C_j^\top v = \lambda C_j C_j^\top v, \quad (4.7)$$

corresponding to the r largest eigenvalues $\lambda_1 \geq \dots \geq \lambda_r \geq 0$, and

$$a_i = -\frac{1}{\|C_j^\top b_i\|^2} S_j^\top R_j C_j^\top b_i \quad i = 1, \dots, r. \quad (4.8)$$

Moreover, the solution $(\mathbf{a}, \mathbf{b}) \in \mathcal{V}_r(m_s, m)$ of (4.6) satisfies

$$\|S_j^\top R_j + \mathbf{a}\mathbf{b}^\top C_j\|_F^2 = \|S_j^\top R_j\|_F^2 - \sum_{i=1}^r \lambda_i. \quad (4.9)$$

Proof. Let \mathcal{O}_j denote the objective function of the minimization problem (4.6), namely $\mathcal{O}_j(\mathbf{a}, \mathbf{b}) := \|S_j^\top R_j + \mathbf{a}\mathbf{b}^\top C_j\|_F^2$. We recast problem (4.6) in the space

$$\widehat{\mathcal{V}}_r(m_s, m) := \{(\mathbf{a}, \mathbf{b}) \in \mathbb{R}^{m_s \times r} \times \mathbb{R}^{m \times r} : \text{rank}(\mathbf{a}) = \text{rank}(\mathbf{b}) = r, \mathbf{a}^\top \mathbf{a} \text{ diagonal}\}.$$

Assume that the pair $(\mathbf{c}, \mathbf{d}) \in \mathcal{V}_r(m_s, m)$ minimizes (4.6), that is

$$(\mathbf{c}, \mathbf{d}) = \arg \min_{(\mathbf{a}, \mathbf{b}) \in \mathcal{V}_r(m_s, m)} \|S_j^\top R_j + \mathbf{a}\mathbf{b}^\top C_j\|_F^2.$$

Let $\mathbf{c} = \mathbf{f}Z$ be the thin QR factorization of \mathbf{c} without normalization, where $\mathbf{f} \in \mathbb{R}^{m_s \times r}$ and $Z \in \mathbb{R}^{r \times r}$ is upper triangular with ones on the main diagonal. Define $\mathbf{g} := \mathbf{d}Z^\top \in \mathbb{R}^{m \times r}$. The rank of \mathbf{g} is r and $\mathbf{f}\mathbf{g}^\top C_j = \mathbf{c}\mathbf{d}^\top C_j$, which implies

$$\min_{(\mathbf{a}, \mathbf{b}) \in \mathcal{V}_r(m_s, m)} \|S_j^\top R_j + \mathbf{a}\mathbf{b}^\top C_j\|_F^2 = \min_{(\mathbf{a}, \mathbf{b}) \in \widehat{\mathcal{V}}_r(m_s, m)} \|S_j^\top R_j + \mathbf{a}\mathbf{b}^\top C_j\|_F^2,$$

and we can restrict our search to the case where the vectors a_i are orthogonal.

In $\widehat{\mathcal{V}}_r$, the objective function can be expanded as

$$\mathcal{O}_j(\mathbf{a}, \mathbf{b}) = \|S_j^\top R_j\|_F^2 + \sum_{i=1}^r \|a_i\|^2 \|C_j^\top b_i\|^2 + 2 \sum_{i=1}^r \text{tr}((S_j^\top R_j)^\top a_i b_i^\top C_j). \quad (4.10)$$

The gradient of (4.10) with respect to the pair of vectors (a_i, b_i) , for any $i = 1, \dots, r$, is given by

$$\nabla_{(a_i, b_i)} \mathcal{O}_j(\mathbf{a}, \mathbf{b}) = \begin{pmatrix} 2 \|C_j^\top b_i\|^2 a_i + 2 S_j^\top R_j C_j^\top b_i \\ 2 \|a_i\|^2 C_j C_j^\top b_i + 2 C_j (S_j^\top R_j)^\top a_i \end{pmatrix}.$$

Imposing the gradient to vanish gives rise to decoupled equations for each pair (a_i, b_i) . In particular, for each $i = 1, \dots, r$, the resulting problem boils down to the rank-1 minimization of [21, Lemma 3.5]. For a fixed index i , a_i is given by (4.8), and b_i is eigenvector of the generalized eigenvalue problem

$$C_j(S_j^\top R_j)^\top (S_j^\top R_j) C_j^\top v = \lambda C_j C_j^\top v.$$

The corresponding eigenvalue $\lambda_i \in \mathbb{R}$ can be written as

$$\lambda_i = \frac{\|S_j^\top R_j C_j^\top b_i\|^2}{\|C_j^\top b_i\|^2}.$$

So far we know that if b_1, \dots, b_r are *any* r eigenvectors of (4.7) and a_1, \dots, a_r are obtained from b_i using (4.8), then $(\mathbf{a}, \mathbf{b}) \in \widehat{\mathcal{V}}_r$ is a stationary point of (4.6).

We now want to identify the global minimum. Starting from (4.10) and inserting the expression for a_i , the second term on the right-hand side becomes

$$\sum_{i=1}^r \|a_i\|^2 \|C_j^\top b_i\|^2 = \sum_{i=1}^r \frac{\|S^\top R C_j^\top b_i\|_2^2}{\|C_j^\top b_i\|^4} \|C_j^\top b_i\|^2 = \sum_{i=1}^r \frac{\|S^\top R C_j^\top b_i\|^2}{\|C_j^\top b_i\|^2} = \sum_{i=1}^r \lambda_i,$$

while the third term is

$$\sum_{i=1}^r \text{tr}((S^\top R)^\top a_i b_i^\top C_j) = \sum_{i=1}^r -\frac{1}{\|C_j^\top b_i\|^2} \text{tr}(b_i^\top C_j (S^\top R)^\top (S^\top R) C_j^\top b_i) = -\sum_{i=1}^r \lambda_i.$$

Hence, the objective function (4.10) in $\widehat{\mathcal{V}}_r$ satisfies (4.9). Since \mathbf{b} is required to have column-rank r , the global minimum of (4.6) is obtained by choosing as b_1, \dots, b_r the eigenvectors of (4.7) corresponding to the r largest eigenvalues. \square

If the matrix C_j does not have full row-rank, that is, $r_C := \text{rank}(C_j) < m$, one can proceed as suggested in [21, Lemma 3.4] by performing a rank-revealing QR decomposition of C_j , i.e., $C_j = Q_j Z_j$ where $Q_j \in \mathbb{R}^{m \times r_C}$ has orthogonal columns and $Z_j \in \mathbb{R}^{r_C \times \bar{w}}$. Introducing the matrix $\mathbf{z} = Q_j^\top \mathbf{b}$, one can use Theorem 4.1 to derive the matrices $(\mathbf{a}, \mathbf{z}) \in \mathcal{V}_r(m_s, r_C)$ that minimize $\|S_j^\top R_j + \mathbf{a} \mathbf{z}^\top Z_j\|_F^2$. The factor \mathbf{b} is then recovered as $\mathbf{b} = Q_j \mathbf{z}$.

The steps to update the DEIM basis are summarized in Algorithm 1.

Algorithm 1 Adaptation of the DEIM projection

- 1: **procedure** $(U_{j+1}, P_{j+1}) = \text{ADAPTBASIS}(\{z^{\ell_{j+1}-w+1}, \dots, z^{\ell_{j+1}}\}, A, U_j, P_j, S_j, r)$
 - 2: Compute the matrix F_j at the interpolation and sampling points: $P_j^\top F_j, S_j^\top F_j$.
 - 3: Compute the DEIM coefficients $C_j = (P_j^\top U_j)^{-1} (P_j^\top F_j)$.
 - 4: Compute the DEIM residual at the sampling points: $S_j^\top R_j = S_j^\top U_j C_j - S_j^\top F_j$.
 - 5: Solve the generalized eigenvalue problem (4.7).
 - 6: Set b_1, \dots, b_r as the eigenvectors corresponding to the r largest eigenvalues.
 - 7: Compute a_1, \dots, a_r using (4.8).
 - 8: Set $\mathbf{a}_j = [a_1 \dots a_r]$ and $\mathbf{b}_j = [b_1 \dots b_r]$.
 - 9: $S_j^\top U_{j+1} \leftarrow S_j^\top U_j + \mathbf{a}_j \mathbf{b}_j^\top$.
 - 10: $\tilde{S}_j^\top U_{j+1} \leftarrow \tilde{S}_j^\top U_j$.
 - 11: Compute the DEIM indices P_{j+1} associated with U_{j+1} .
 - 12: **end procedure**
-

For each value of the parameter, the complexity of updating the DEIM basis, as described in Algorithm 1, is $O(m_s k w (s_1 + s_2)) + O(m^2 m_s) + O(m_s m k w)$. In greater detail, under the assumption that the Jacobian $J_{\eta, h}$ has at most $s_1 + s_2$ non-zero entries per row, the computation of $P_j^\top F_j = P_j^\top J_{\eta, h}(A z^i) A$ for all w hyper-reduced solutions z^i in the temporal window leads to a computational cost of the order of $O((s_1 + s_2) m k w)$. Analogously, with m_s instead of m , $S_j^\top F_j \in \mathbb{R}^{m_s \times \bar{w}}$ requires $O((s_1 + s_2) m_s k w)$ operations. Next, the matrix-matrix multiplications involved in the computation of $C_j \in \mathbb{R}^{m \times \bar{w}}$ (line 3) and of $S_j^\top R_j \in \mathbb{R}^{m_s \times \bar{w}}$ (line 4) require $O(m^3) + O(m^2 k w) + O(m_s m k w)$ operations. The computation of the matrix $C_j (S_j^\top R_j)^\top (S_j^\top R_j) C_j^\top$ and the solution of the generalized

eigenvalue problem (4.7) have arithmetic complexity $O(m_s m k w) + O(m^2 m_s) + O(m^3)$. Finally, the total complexity of computing the matrix $\mathbf{a} \in \mathbb{R}^{m_s \times r}$ via (4.8) is $O(r m m_s + r m k w)$.

The update of the DEIM interpolation points (line 11) can be performed, for example, by means of the greedy algorithm described in [7] and whose complexity is $O(m^3) + O(m^2 d)$, cf. [9]. This cost is linear in d because, at each iteration of [7, Algorithm 1], the norm of the d -dimensional DEIM residual needs to be computed. To reduce the computational burden of this step, in [21, Section 4.1], the authors suggest to update only the indices associated with the DEIM basis vectors that have undergone the largest rotations in the DEIM basis update from U_j to U_{j+1} .

4.2 Sampling points update

A crucial aspect of Algorithm 1 is the definition of the sampling matrix S_j at each update. In this section, we study how to determine the best possible choice of sampling points by analyzing the reduction in the residual associated with the DEIM update and the distance of the DEIM space to the best approximation space at a given time. To this end, we first show that the DEIM update minimizes the projection error of the residual at the sampling points onto the space spanned by the rows of C_j .

Lemma 4.2. *Let \bar{r} be the rank of the matrix $S_j^\top R_j C_j^\top \in \mathbb{R}^{m_s \times m}$ and assume that the DEIM coefficient matrix $C_j \in \mathbb{R}^{m \times \bar{w}}$ has full row-rank. Let U_{j+1} be the rank- \bar{r} update given by Algorithm 1. Then,*

$$\|S_j^\top (U_{j+1} C_j - F_j)\|_F = \|S_j^\top R_j (I - \mathbb{C}_j)\|_F,$$

where $\mathbb{C}_j = C_j^\top (C_j C_j^\top)^{-1} C_j \in \mathbb{R}^{\bar{w} \times \bar{w}}$.

Proof. For all $i = 1, \dots, \bar{r}$, the eigenpairs (λ_i, b_i) satisfy the generalized eigenvalue problem (4.7), namely

$$C_j (S_j^\top R_j)^\top (S_j^\top R_j) C_j^\top \mathbf{b} = C_j C_j^\top \mathbf{b} \Lambda, \quad (4.11)$$

where $\Lambda = \text{diag}(\lambda_1, \dots, \lambda_{\bar{r}})$. Since C_j has full row-rank, the matrix $C_j C_j^\top$ is symmetric and positive definite, thus admitting the Cholesky decomposition $C_j C_j^\top = L_j L_j^\top$, where $L_j \in \mathbb{R}^{m \times m}$ is lower triangular. We introduce the change of variables $\mathbf{c} = L_j^\top \mathbf{b}$, so that (4.11) becomes

$$L_j^{-1} C_j (S_j^\top R_j)^\top (S_j^\top R_j) C_j^\top L_j^{-\top} \mathbf{c} = \mathbf{c} \Lambda.$$

This means that the eigenvalues of the generalized problem (4.7) coincide with the squared singular values of the matrix $M_j := S_j^\top R_j C_j^\top L_j^{-\top} \in \mathbb{R}^{m_s \times m}$. Then, equation (4.9) can be written as

$$\|S_j^\top R_j + \mathbf{a} \mathbf{b}^\top C_j\|_F^2 = \|S_j^\top R_j\|_F^2 - \sum_{\ell=1}^{\bar{r}} \sigma_\ell^2, \quad (4.12)$$

where $\sigma_1 \geq \sigma_2 \geq \dots \geq \sigma_{\bar{r}} > 0$ are the singular values of M_j . In particular, since $\bar{r} = \text{rank}(S_j^\top R_j C_j^\top)$, then

$$\|S_j^\top R_j + \mathbf{a} \mathbf{b}^\top C_j\|_F^2 = \|S_j^\top R_j\|_F^2 - \|S_j^\top R_j C_j^\top L_j^{-\top}\|_F^2.$$

Moreover, by the cyclic property of the trace, it holds

$$\|S_j^\top R_j\|_F^2 - \|S_j^\top R_j C_j^\top L_j^{-\top}\|_F^2 = \text{tr}((I - C_j^\top (C_j C_j^\top)^{-1} C_j)(S_j^\top R_j)^\top (S_j^\top R_j)).$$

Since $\mathbb{C}_j = \mathbb{C}_j^\top$ and $\mathbb{C}_j^2 = \mathbb{C}_j$, we have $I - \mathbb{C}_j = (I - \mathbb{C}_j)(I - \mathbb{C}_j)^\top$, and

$$\|S_j^\top R_j + \mathbf{a} \mathbf{b}^\top C_j\|_F^2 = \text{tr}((I - \mathbb{C}_j)(I - \mathbb{C}_j)^\top (S_j^\top R_j)^\top (S_j^\top R_j)),$$

which concludes the proof. \square

The number of non-zero eigenvalues in the generalized eigenvalue problem (4.7) coincides with the number \bar{r} of non-zero singular values of $S_j^\top R_j C_j^\top L_j^{-\top}$. Furthermore, owing to (4.12), including eigenvectors of (4.7) corresponding to zero eigenvalues as columns of \mathbf{b} will have no effect on the value of the objective function (4.6). This suggests that the rank r of the update should be chosen so that $r \leq \bar{r}$.

In the following result we study the distance between the DEIM space resulting from the update described in Algorithm 1 and the best possible approximation space, namely the one spanned by the columns of F_j , for any $j = 0, \dots, N_a$. The resulting bound gives us an indication on how the sampling matrix can be chosen to minimize this error. Note that the result derived in the following theorem is analogous to [20, Proposition 2].

Theorem 4.3. *Assume that the DEIM coefficient matrix $C_j \in \mathbb{R}^{m \times \bar{w}}$ has full row-rank. Let $U_{j+1} = U_j + \alpha_j \beta_j^\top$ be the rank- \bar{r} update of U_j obtained with Algorithm 1. Let \mathcal{U}_{j+1} be the space spanned by the columns of U_{j+1} , and let the columns of F_j belong to the m -dimensional space $\bar{\mathcal{U}}_{j+1}$. Then, the distance between $\bar{\mathcal{U}}_{j+1}$ and \mathcal{U}_{j+1} is bounded as*

$$d(\bar{\mathcal{U}}_{j+1}, \mathcal{U}_{j+1}) := \|\bar{U}_{j+1} - U_{j+1} U_{j+1}^\top \bar{U}_{j+1}\|_F^2 \leq \frac{\rho_j^2}{\sigma_{\min}(F_j)} \quad (4.13)$$

where $\sigma_{\min}(F_j)$ is the smallest nonzero singular value of F_j and

$$\rho_j^2 := \|R_j(I - \mathbb{C}_j)\|_F^2 + \|\check{S}_j^\top R_j \mathbb{C}_j\|_F^2 = \|R_j\|_F^2 - \|S_j^\top R_j \mathbb{C}_j\|_F^2.$$

Proof. First note that the update $\alpha_j \beta_j^\top$ only changes the rows of U_j corresponding to the sampling points S_j as shown in (4.5). Lemma 4.2 yields

$$\begin{aligned} \|U_{j+1} C_j - F_j\|_F^2 &= \|S_j^\top (U_{j+1} C_j - F_j)\|_F^2 + \|\check{S}_j^\top (U_{j+1} C_j - F_j)\|_F^2 \\ &= \|S_j^\top R_j (I - \mathbb{C}_j)\|_F^2 + \|\check{S}_j^\top R_j\|_F^2 \\ &= \|R_j(I - \mathbb{C}_j)\|_F^2 - \|\check{S}_j^\top R_j(I - \mathbb{C}_j)\|_F^2 + \|\check{S}_j^\top R_j\|_F^2. \end{aligned} \quad (4.14)$$

The linearity and cyclic property of the trace, together with the fact that \mathbb{C}_j is a projection, give $\|\check{S}_j^\top R_j\|_F^2 - \|\check{S}_j^\top R_j(I - \mathbb{C}_j)\|_F^2 = \|\check{S}_j^\top R_j \mathbb{C}_j\|_F^2$. Hence, equation (4.14) yields $\|U_{j+1} C_j - F_j\|_F^2 = \rho_j^2$.

Let \bar{U}_{j+1} be an orthonormal basis matrix of $\bar{\mathcal{U}}_{j+1}$. Since the columns of F_j belong to $\bar{\mathcal{U}}_{j+1}$, there is a matrix $\tilde{F}_j \in \mathbb{R}^{m \times \bar{w}}$ such that $F_j = \bar{U}_{j+1} \tilde{F}_j$. Hence,

$$\begin{aligned} \|F_j - U_{j+1} U_{j+1}^\top F_j\|_F^2 &= \|(\bar{U}_{j+1} - U_{j+1} U_{j+1}^\top \bar{U}_{j+1}) \tilde{F}_j\|_F^2 \\ &\geq \|\bar{U}_{j+1} - U_{j+1} U_{j+1}^\top \bar{U}_{j+1}\|_F^2 \sigma_{\min}^2(\tilde{F}_j), \end{aligned} \quad (4.15)$$

and $\sigma_{\min}(\tilde{F}_j) = \sigma_{\min}(F_j)$ since \bar{U}_{j+1} is orthonormal. Combining (4.15) with the bound

$$\|F_j - U_{j+1} U_{j+1}^\top F_j\|_F^2 \leq \|F_j - U_{j+1} C_j\|_F^2,$$

due to the fact that U_{j+1} is an orthonormal basis of \mathcal{U}_{j+1} , yields the conclusion. \square

If $\rho_j = 0$ in (4.13), then the spaces \mathcal{U}_{j+1} and $\bar{\mathcal{U}}_{j+1}$ coincide, and the adapted DEIM basis U_{j+1} can exactly represent all snapshots F_j of the reduced Jacobian in the window. This observation suggests that the ideal set of sample indices S_j is the one that minimizes ρ_j . In particular, since R_j and \mathbb{C}_j are fixed, we choose the S_j that minimizes $\|\check{S}_j^\top R_j \mathbb{C}_j\|_F$ or, equivalently, maximizes $\|S_j^\top R_j \mathbb{C}_j\|_F$.

We remark the adaptive method proposed in [20] is based on a different update of the DEIM basis, performed via SVD of the residual matrix R_j (see [20, Algorithm 3]). Similarly, the sampling matrix S_j is chosen to minimize $\|\check{S}_j^\top R_j\|_F$.

We summarize the steps for the adaptation of the sampling indices in Algorithm 2.

Algorithm 2 Adaptation of the sampling indices

```

1: procedure  $S_{j+1} = \text{ADAPTSAMPLEINDICES}(\{z^{\ell_{j+1}-w+1}, \dots, z^{\ell_{j+1}}\}, A, U_j, P_j, m_s)$ 
2:   Build the snapshot matrix  $F_j$  of the reduced Jacobian in the window.
3:   Compute  $R_j \mathbb{C}_j = U_j C_j - F_j C_j^\top (C_j C_j^\top)^{-1} C_j$ .
4:   Take as new sampling indices the indices of the  $m_s$  rows of  $R_j \mathbb{C}_j$  with largest norm.
5: end procedure

```

To analyze the computational cost of Algorithm 2, we first observe that some of the quantities involved are already available from the basis update described in Algorithm 1. The operations required are the computation of the $d - m$ entries of F_j not available from $P_j^\top F_j$, at a cost of order $O((d - m)kw(s_1 + s_2))$. To construct \mathbb{C}_j one can use the SVD of $C_j = \mathcal{U}_j \Sigma_j \mathcal{V}_j^\top$ so that $\mathbb{C}_j = \tilde{\mathcal{V}}_j \tilde{\mathcal{V}}_j^\top$, where $\tilde{\mathcal{V}}_j \in \mathbb{R}^{w \times m}$ is obtained by selecting the first m columns of \mathcal{V}_j . In this case, $R_j \mathbb{C}_j = U_j C_j - F_j \tilde{\mathcal{V}}_j \tilde{\mathcal{V}}_j^\top$ can be computed with $O(dmkw)$ operations. The arithmetic complexity of Algorithm 2 is then $O((d - m)kw(s_1 + s_2)) + O(dmkw)$, which is linear in d . Since this quantity typically scales with the full dimension n (see discussion in Remark 3.1), the update of the sampling indices turns out to be too expensive to be performed at each adaptation step. In particular, solving the adaptive hyper-reduced system may become computationally demanding for large values of w or m , as observed in the numerical experiments, Table 8 and Figure 11 in particular. For this reason, as suggested in [20, Section 3.4.1], it is preferable to perform the update of the sampling indices every γ steps, where $\gamma = \nu\delta$ and $\nu > 1$. Moreover, instead of being fixed *a priori*, the number of sampling indices m_s may be determined at each adaptation based on a stopping tolerance, so that indices are included until $\|\tilde{S}_j R_j \mathbb{C}_j\|_F$ is sufficiently small. We refer to Section 5.2.2 for a numerical study regarding these aspects.

The gradient-preserving adaptive DEIM scheme is summarized in Algorithm 3.

Algorithm 3 Gradient-preserving adaptive DEIM

```

1: procedure GP-ADEIM( $A, \delta_0, \delta, w, \gamma, m_s, r$ )
2:   Compute  $(U_0, P_0)$  from snapshots  $J_{\eta, h}(AA^\top y^\ell(\eta))$  for  $\ell = 0, \dots, \delta_0$ .
3:    $j \leftarrow 0$ 
4:   for  $\tau = 1, \dots, N_t - 1$  do
5:     Compute  $z^\tau$  by solving (4.1) with  $U_j$  and  $P_j$ .
6:     if  $\text{mod}(\tau - \delta_0, \delta) = 0$  then
7:       Collect reduced trajectories in the window:  $\mathcal{Z} = \{z^{\delta_0 + j\delta - w + 1}, \dots, z^{\delta_0 + j\delta}\}$ .
8:       if  $\text{mod}(\tau - \delta_0, \gamma) = 0$  then
9:          $S_j \leftarrow \text{ADAPTSAMPLEINDICES}(\mathcal{Z}, A, U_j, P_j, m_s)$  with Algorithm 2.
10:      else
11:         $S_j \leftarrow S_{j-1}$ 
12:      end if
13:       $(U_{j+1}, P_{j+1}) \leftarrow \text{ADAPTBASIS}(\mathcal{Z}, A, U_j, P_j, S_j, r)$  with Algorithm 1.
14:       $j \leftarrow (\tau - \delta_0)/\delta + 1$ 
15:    end if
16:   end for
17: end procedure

```

4.3 Conservation of the Hamiltonian

Similarly to the study conducted in Section 3.3 for the non-adaptive hyper-reduction algorithm, we assess the error that we introduce in the conservation of the Hamiltonian by approximating it via a *local* hyper-reduction. In the following result we show that the error between the Hamiltonian

evaluated at the full model solution and at the hyper-reduced solution at a given time is bounded by the sum of the local hyper-reduction error of h at all previous updates.

Proposition 4.4. *Let $\eta \in \mathcal{P}$ be fixed. Let $y^{\ell_j}(\eta)$ be an approximation of the solution $y(t^{\ell_j}, \eta)$ of the full order system (2.1) at time t^{ℓ_j} , with $j = 1, \dots, N_a + 1$, obtained with a user-defined numerical time integrator. Similarly, let $z^{\ell_j}(\eta)$ be an approximation of the solution $z(t^{\ell_j}, \eta)$ of the hyper-reduced system (3.5) at time t^{ℓ_j} . Assume that $y^0(\eta) \in \text{Col}(A)$ and $h(AA^\top y^0(\eta), \eta) \in \text{Col}(U_0)$. Furthermore, assume that the basis is updated so that $h(Az^{\ell_j}(\eta), \eta) \in \text{Col}(U_j)$ for all $j = 1, \dots, N_a$. Then, the error $\Delta\mathcal{H}_j(\eta) := |\mathcal{H}(y^{\ell_j}(\eta), \eta) - \mathcal{H}(Az^{\ell_j}(\eta), \eta)|$ satisfies*

$$\Delta\mathcal{H}_j(\eta) \leq \sum_{i=0}^{j-1} (|v^\top(I - \mathbb{P}_i)h(Az^{\ell_{i+1}}(\eta), \eta)| + \varepsilon_{\mathcal{H}_{hr}^i}^{[t^{\ell_i}, t^{\ell_{i+1}}]}) + \varepsilon_{\mathcal{H}}^{[t^0, t^{\ell_j}]},$$

where $\varepsilon_{\mathcal{H}_{hr}^j}^{[t^{\ell_j}, t^{\ell_{j+1}}]} := |\mathcal{H}_{hr}^j(z^{\ell_{j+1}}) - \mathcal{H}_{hr}^j(z^{\ell_j})|$ and $\varepsilon_{\mathcal{H}}^{[t^0, t^{\ell_j}]} := |\mathcal{H}(y^{\ell_j}) - \mathcal{H}(y^0)|$ are the errors in the Hamiltonian conservation in the specified interval and associated with the chosen temporal integrator.

Proof. In this proof we omit the dependence of y^{ℓ_j} , z^{ℓ_j} , and of \mathcal{H} on η . The Hamiltonian error at the generic time instant t^{ℓ_j} can be bounded as

$$\Delta\mathcal{H}_j(\eta) \leq |\mathcal{H}(y^{\ell_j}) - \mathcal{H}(y^0)| + |\mathcal{H}(y^0) - \mathcal{H}(Az^0)| + |\mathcal{H}(Az^0) - \mathcal{H}(Az^{\ell_j})|.$$

The first term on the right-hand side is $\varepsilon_{\mathcal{H}}^{[t^0, t^{\ell_j}]}$ and only depends on the time integration scheme. Moreover, the second term is zero since $y^0 \in \text{Col}(A)$ by assumption. As shown in Section 3.3, equation (3.17), this assumption can be easily enforced by a suitable shift of the initial condition. The third term can be bounded as

$$\begin{aligned} |\mathcal{H}(Az^0) - \mathcal{H}(Az^{\ell_j})| &\leq |\mathcal{H}(Az^0) - \mathcal{H}_{hr}^0(z^0)| + \sum_{i=0}^{j-1} |\mathcal{H}_{hr}^i(z^{\ell_{i+1}}) - \mathcal{H}_{hr}^i(z^{\ell_i})| \\ &\quad + \sum_{i=0}^{j-2} |\mathcal{H}_{hr}^{i+1}(z^{\ell_{i+1}}) - \mathcal{H}_{hr}^i(z^{\ell_{i+1}})| + |\mathcal{H}_{hr}^{j-1}(z^{\ell_j}) - \mathcal{H}(Az^{\ell_j})|. \end{aligned}$$

The first term on the right-hand side vanishes if $h(Az^0) \in \text{Col}(U_0)$. Furthermore, the quantity $|\mathcal{H}_{hr}^i(z^{\ell_i}) - \mathcal{H}_{hr}^i(z^{\ell_{i+1}})| = \varepsilon_{\mathcal{H}_{hr}^i}^{[t^{\ell_i}, t^{\ell_{i+1}}]}$ only depends on the temporal integrator. The third term can be further split as follows, for all $i = 0, \dots, j-2$,

$$|\mathcal{H}_{hr}^i(z^{\ell_{i+1}}) - \mathcal{H}_{hr}^{i+1}(z^{\ell_{i+1}})| \leq |\mathcal{H}_{hr}^i(z^{\ell_{i+1}}) - \mathcal{H}(Az^{\ell_{i+1}})| + |\mathcal{H}(Az^{\ell_{i+1}}) - \mathcal{H}_{hr}^{i+1}(z^{\ell_{i+1}})|,$$

where the second term vanishes if $h(Az^{\ell_{i+1}}) \in \text{Col}(U_{i+1})$.

The conclusion follows from the definition of the full order and hyper-reduced Hamiltonian. \square

Observe that, whenever $h(Az^{\ell_j})$ is not in the column space of the updated basis U_j , the error $|\mathcal{H}(Az^{\ell_j}) - \mathcal{H}_{hr}^j(z^{\ell_j})|$ does not vanish. In practice, this error is of the same order as the DEIM projection error $|v^\top(I - \mathbb{P}_j)h(Az^{\ell_{j+1}}(\eta), \eta)|$ and, hence, does not play a role in the global conservation of the Hamiltonian, as observed in the numerical experiments, see e.g. Table 11.

5 Numerical experiments

To numerically assess the performances of the proposed methods, we consider two one-dimensional problems: the shallow water equations and the nonlinear Schrödinger equation. As numerical time integration schemes we compare the implicit midpoint rule (IMR), which is a symplectic time

integrator [13], and the Average Vector Field (AVF), which is not symplectic but it exactly preserves the Hamiltonian [24, 5]. The tolerance of the Newton method used within the implicit timestepping is set to 10^{-10} .

In all the numerical tests, we assess the accuracy of the reduced and hyper-reduced solutions by means of the following errors:

$$\mathcal{E}_{L^2} = \sqrt{\Delta t} \sqrt{\sum_{i=1}^{N_t} \|y^i - Az^i\|^2}, \quad \mathcal{E}_{\text{fin}} = \|y^{N_t} - Az^{N_t}\|. \quad (5.1)$$

We shall distinguish between $\mathcal{E}_{L^2}^R$, $\mathcal{E}_{\text{fin}}^R$ and $\mathcal{E}_{L^2}^{\text{HR}}$, $\mathcal{E}_{\text{fin}}^{\text{HR}}$ according to whether z^i is the reduced or the hyper-reduced solution at time t^i , respectively.

5.1 Shallow water equations

The one-dimensional shallow water equations [25] read

$$\begin{cases} \partial_t \chi + \partial_x ((1 + \chi) \partial_x \Phi) = 0, & x \in [-L, L], t \in (0, T], \\ \partial_t \Phi + \frac{1}{2} (\partial_x \Phi)^2 + \chi = 0, & x \in [-L, L], t \in (0, T], \end{cases} \quad (5.2)$$

where ∂_t and ∂_x are short-hand notations for the temporal and spatial derivative, respectively; $1 + \chi$ is the height of the free surface, normalized by its mean value, and $\chi = \chi(x, t; \eta)$ is the perturbation from the equilibrium position; $\Phi = \Phi(x, t; \eta)$ is the scalar velocity potential, that is, $\partial_x \Phi$ is the horizontal velocity normalized by the characteristic speed $\sqrt{g(1 + \chi)}$, with g the acceleration of gravity. We complement the problem with periodic boundary conditions and initial conditions.

Problem (5.2) admits a Hamiltonian formulation with Hamiltonian

$$\widehat{\mathcal{H}}(\chi, \Phi) = \frac{1}{2} \int_{-L}^L ((1 + \chi) (\partial_x \Phi)^2 + \chi^2) \, dx.$$

We discretize the spatial differential operators in (5.2) using centered second-order finite differences. To this end, we introduce a uniform mesh on the domain $[-L, L]$ with $x_i = -L + i\Delta x$, for $i = 0, \dots, n$ and $\Delta x = 2L/n$. Let $D_x \in \mathbb{R}^{n \times n}$ be the matrix corresponding to the finite-difference discretization of the spatial derivative. Defining the vectors $\boldsymbol{\chi}(t, \eta) = (\chi_1, \dots, \chi_n)^\top$, and $\boldsymbol{\Phi}(t, \eta) = (\Phi_1, \dots, \Phi_n)^\top$, where χ_i and Φ_i are approximations of $\chi(x_i)$ and $\Phi(x_i)$, we obtain the discretized system

$$\begin{cases} \dot{\boldsymbol{\chi}} + D_x^2 \boldsymbol{\Phi} + D_x(\boldsymbol{\chi} \odot D_x \boldsymbol{\Phi}) = \mathbf{0}, \\ \dot{\boldsymbol{\Phi}} + \boldsymbol{\chi} + \frac{1}{2} (D_x \boldsymbol{\Phi}) \odot (D_x \boldsymbol{\Phi}) = \mathbf{0}. \end{cases}$$

Here, the symbol \odot denotes the pointwise product of vectors. This is a Hamiltonian system of the form (2.1) with $y(t, \eta) = (\boldsymbol{\chi}^\top(t, \eta), \boldsymbol{\Phi}^\top(t, \eta))^\top \in \mathbb{R}^{2n}$ and

$$\mathcal{N}(y) = \frac{1}{2} \sum_{i=1}^n \chi_i (D_x \boldsymbol{\Phi})_i^2 = v^\top h(y),$$

where $v \in \mathbb{R}^n$ is the vector having all entries equal to one and $h(y) \in \mathbb{R}^n$ is defined as $(h(y))_i := \frac{1}{2} \chi_i (D_x \boldsymbol{\Phi})_i^2$ for all $i = 1, \dots, n$. Notice that, in this case, the decomposition of h is such that $d = n$.

In the following experiments we set $L = 10$ and $n = 2000$ grid points, corresponding to $\Delta x = 0.01$. The final time is set to $T = 7$ and the time step is $\Delta t = 0.001$. The initial condition is $\boldsymbol{\Phi}(x, 0) = 0$, while the vertical displacement χ is a Gaussian profile of the form $\chi(x, 0; \eta) = \alpha e^{-\beta x^2}$, where $\eta = (\alpha, \beta)$ is the problem parameter and it ranges in the set $\mathcal{P} = [\frac{1}{10}, \frac{1}{7}] \times [\frac{1}{5}, \frac{3}{2}] \subset \mathbb{R}^2$. The shift described in Section 3.3 is performed on the initial condition.

For this test case, we compare the performances of the full model, the reduced model and the hyper-reduced model obtained with the non-adaptive algorithm.

To construct the reduced model, the full system is solved, in the offline phase, for 4 equispaced values of α and β , for a total of 16 training parameters. The computational time required to solve the full order system with AVF for every instance of the parameter is approximately 9 minutes. Next, the reduced basis is built via complex SVD using all N_t temporal snapshots for every training parameter. We choose two different dimensions of the reduced space, namely $2k = 80$ and $2k = 160$. For the hyper-reduced problem, we build the DEIM basis via POD on snapshots of the reduced Jacobian collected every 40 time steps for every training parameter.

We test the reduced model (2.3) and the hyper-reduced model (3.5) for the parameter $\eta = (4/35, 16/15) \notin \Gamma_s$, that is, the midpoint of the parameter space \mathcal{P} . In Figure 1 we report the errors (5.1) of the hyper-reduced model vs. the size m of the DEIM basis, obtained with the AVF and IMR time integrators and for the two sizes $2k \in \{80, 160\}$ of the reduced space. As expected, the error of the hyper-reduced solution converges to the error of the reduced solution as m increases. Moreover, as the size $2k$ of the reduced model increases, a larger number of DEIM bases are required to approach the limit value. The errors obtained with the two numerical time integration schemes are very similar.

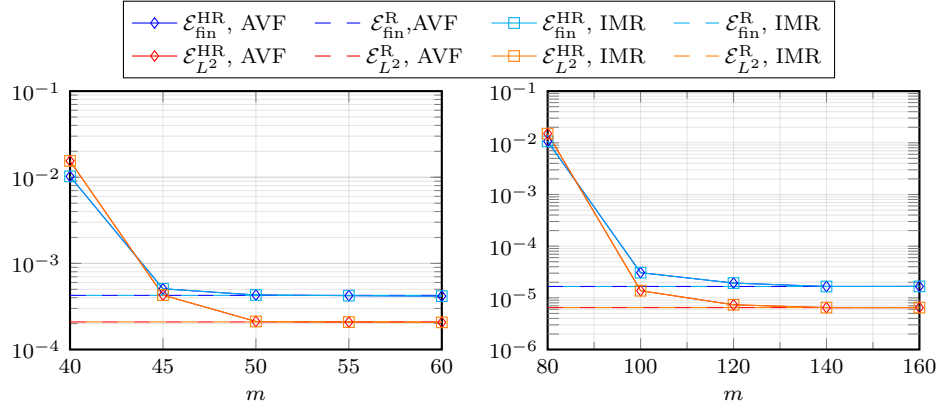


Figure 1: Shallow water equations. Errors (5.1) of the reduced and hyper-reduced models vs. size m of the DEIM space. The size of the reduced model is $2k = 80$ (left) and $2k = 160$ (right). Comparison of AVF and IMR for time integration.

The computational times required by the reduced and hyper-reduced models solved using the AVF time integrator are reported in Table 1. The cost of solving the hyper-reduced problem is reduced by a factor of 90 for $2k = 80$ with respect to the reduced model, and by a factor of 25 when $2k = 160$. For the IMR time stepping, no significant differences were recorded in terms of computational time with respect to the AVF simulations.

Observe that, in the case $2k = 160$, the hyper-reduced model with $m = 140$ is as accurate as the reduced model but it is more than 25 times faster to solve.

Table 1: Shallow water equations. Computational times of the online phases of the reduced and hyper-reduced systems, $2k = 80$ (top) and $2k = 160$ (bottom). The test parameter is $\eta = (4/35, 16/15) \notin \Gamma_s$. AVF is used as time integrator. The reported times are computed as averages over 5 runs.

Reduced model $2k = 80$	$m = 40$	$m = 45$	$m = 50$	$m = 55$	$m = 60$
8 min 25 s	4.97 s	5.20 s	5.29 s	5.62 s	5.54 s
Reduced model $2k = 160$	$m = 80$	$m = 100$	$m = 120$	$m = 140$	$m = 160$
9 min 40 s	18.22 s	19.12 s	20.74 s	21.22 s	23.31 s

We then focus on the conservation of the Hamiltonian for a fixed parameter $\eta = (4/35, 16/15)$, whose dependence we omit in the following. In particular, we monitor the error $|\mathcal{H}(y^0) - \mathcal{H}(Az^j)|$ for all time indices $j = 0, \dots, N_t$. This quantity, in turn, is bounded by the error $\Delta\mathcal{H}_j$ in approximating the reduced Hamiltonian with the hyper-reduced one: as derived in Section 3.3, it holds

$$|\mathcal{H}(y^0) - \mathcal{H}(Az^j)| \leq \varepsilon_{\mathcal{H}}^{[t^0, t^j]} + \Delta\mathcal{H}_j \quad \text{for all } j = 0, \dots, N_t. \quad (5.3)$$

Figure 2 shows the three terms involved in the bound at every time instant t^j when the dimension of the reduced space is $2k = 160$. We consider both AFV (left) and IMR (right) for time integration. The error $\varepsilon_{\mathcal{H}}^{[t^0, t^j]}$ in the conservation of the full order Hamiltonian (black line in Figure 2) only depends on the timestepping. We observe that, although IMR is not guaranteed to exactly preserve the Hamiltonian, we record an error of the order of 10^{-11} . Concerning the other terms, we observe that the error in the conservation of the Hamiltonian associated with the hyper-reduced model decreases as m increases, that is, as the quality of the approximation of the Hamiltonian improves. For m sufficiently large, in this test case $m \geq 140$, the error due to the time integration is dominating over the error introduced by the Hamiltonian hyper-reduction. The reason is that the hyper-reduced model with $m \geq 140$ is as accurate as the reduced model and, hence, the Hamiltonian is exactly preserved up to the error of the temporal integrator.

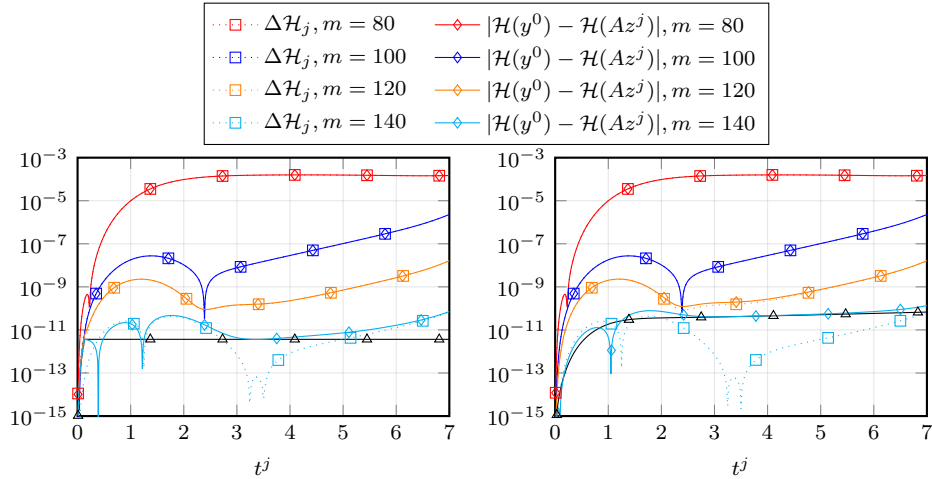


Figure 2: Shallow water equations. Conservation of the Hamiltonian over time for different choices of the DEIM basis m . The solid black lines with triangular marks corresponds to the error $\varepsilon_{\mathcal{H}}^{[t^0, t^j]}$ of the full Hamiltonian due to the timestepping. AVF (left) and IMR (right) for time integration. The reduced model has dimension $2k = 160$ and the test parameter is $\eta = (4/35, 16/15) \notin \Gamma_s$.

As a further confirmation of the relationship between the conservation and the hyper-reduction of the Hamiltonian stated in Proposition 3.5, we plot in Figure 3 the error $\Delta\mathcal{H}_j$ and the DEIM approximation error $|\mathcal{H}_{hr}(z^j) - \mathcal{H}(Az^j)| = |v^\top(\mathbb{P}h(Az^j) - h(Az^j))|$ for all $j = 0, \dots, N_t$. It is worth pointing out that, although the DEIM projection \mathbb{P} is designed to approximate the Jacobian of h , it yields an accurate approximation of h as well.

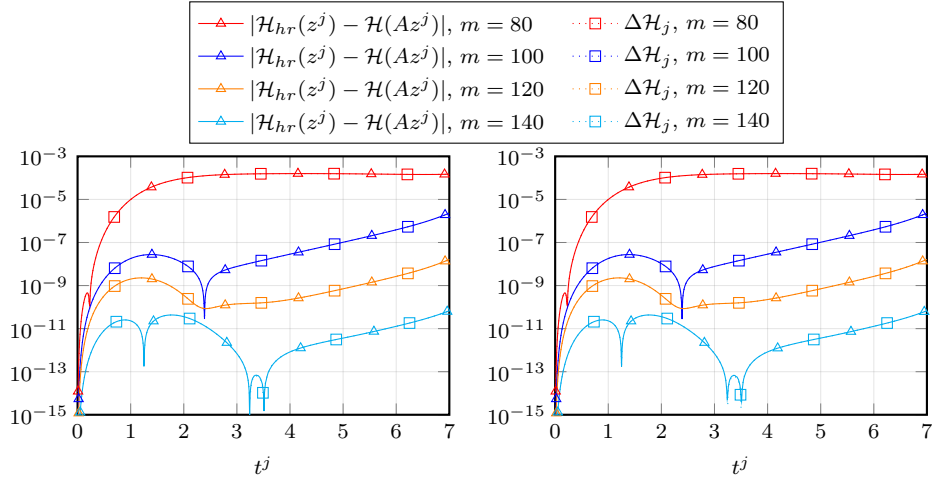


Figure 3: Shallow water equations. Evolution of the approximation error of Hamiltonian for different choices of the DEIM basis m . AVF (left) and IMR (right) for time integration. The reduced model has dimension $2k = 160$ and the test parameter is $\eta = (4/35, 16/15) \notin \Gamma_s$.

5.2 Nonlinear Schrödinger equation

As a second test case, we consider the nonlinear Schrödinger equation

$$\imath \partial_t u + \partial_{xx} u + \epsilon |u|^2 u = 0, \quad x \in [-L, L], t \in (0, T], \quad (5.4)$$

with initial condition $u(x, 0; \eta) = \sqrt{2}(\cosh x)^{-1} \exp(\imath \frac{x}{2})$ and periodic boundary conditions. Here ∂_{xx} denotes the second order derivative with respect to the spatial variable, and $\epsilon = \eta \in \mathbb{R}$ is a parameter ranging in the set $\mathcal{P} = [0.9, 1.1]$. Writing $u(x, t; \eta) = q(x, t; \eta) + \imath p(x, t; \eta)$, for all $(x, t) \in [-L, L] \times [0, T]$, problem (5.4) admits a Hamiltonian formulation with Hamiltonian

$$\hat{\mathcal{H}}(q, p) = \frac{1}{2} \int_{-L}^L \left((\partial_x p)^2 + (\partial_x q)^2 - \frac{\epsilon}{2} (q^2 + p^2)^2 \right) dx.$$

We discretize (5.4) by means of a finite difference scheme on the uniform computational grid $x_i = -L + i\Delta x$, for $i = 0, \dots, n$ and $\Delta x = 2L/n$. Let $D_{xx} \in \mathbb{R}^{n \times n}$ be the matrix corresponding to the finite-difference discretization of the second order spatial derivative. Introducing the vectors $\mathbf{q}(t, \eta) = (q_1, \dots, q_n)^\top$ and $\mathbf{p}(t, \eta) = (p_1, \dots, p_n)^\top$, where q_i and p_i are approximations to $q(x_i)$ and $p(x_i)$, we derive the system

$$\begin{cases} \dot{\mathbf{q}} = -D_{xx}\mathbf{p} - \epsilon(\mathbf{q}^2 + \mathbf{p}^2) \odot \mathbf{p}, \\ \dot{\mathbf{p}} = D_{xx}\mathbf{q} + \epsilon(\mathbf{q}^2 + \mathbf{p}^2) \odot \mathbf{q}, \end{cases}$$

which is of the form (2.1) with $y(t, \eta) = (\mathbf{q}^\top(t, \eta), \mathbf{p}^\top(t, \eta))^\top \in \mathbb{R}^{2n}$ and

$$\mathcal{N}(y) = -\frac{\epsilon}{4} \sum_{i=1}^n (q_i^2 + p_i^2)^2 = v^\top h(y).$$

Here $v \in \mathbb{R}^n$ is the vector with entries all equal to one and $h(y) \in \mathbb{R}^n$ is defined as $(h(y))_i := -\frac{\epsilon}{4}(q_i^2 + p_i^2)^2$ for all $i = 1, \dots, n$. In the following tests we set $L = \pi/l$ with $l = 0.11$ as in [1] and $n = 2048$. AVF and IMR time integrators are applied in the temporal interval $[0, 30]$ with time step $\Delta t = 0.01$, which corresponds to $N_t = 3000$ time steps.

To construct the reduced model, we take snapshots of the full model solution at each time step and for $|\Gamma_s| = 11$ equispaced training parameters in the interval $\mathcal{P} = [0.9, 1.1]$. Each simulation of the

full model takes about 32 minutes. The reduced basis is built using the complex SVD; we consider dimensions $2k = 200$ and $2k = 400$.

In the following sections we compare the performances of the proposed hyper-reduction methods using the non-adaptive and adaptive algorithms for the construction of the DEIM approximation. We use as test parameter $\eta = 1.0932 \notin \Gamma_s$.

5.2.1 Non-adaptive hyper-reduction algorithm

In the non-adaptive hyper-reduction, the DEIM basis is constructed offline from snapshots of the reduced Jacobian. In particular, we consider one snapshot every 20 time steps for each training parameter. The hyper-reduced system is then solved for different values m of the size of the DEIM approximation space. In Figure 4 we report the errors (5.1) of the hyper-reduced model vs. the size m of the DEIM basis, obtained with the AVF and IMR time integrators and for the two sizes $2k \in \{200, 400\}$ of the reduced space. As expected, the error of the hyper-reduced solution converges to the error of the reduced solution as m increases.

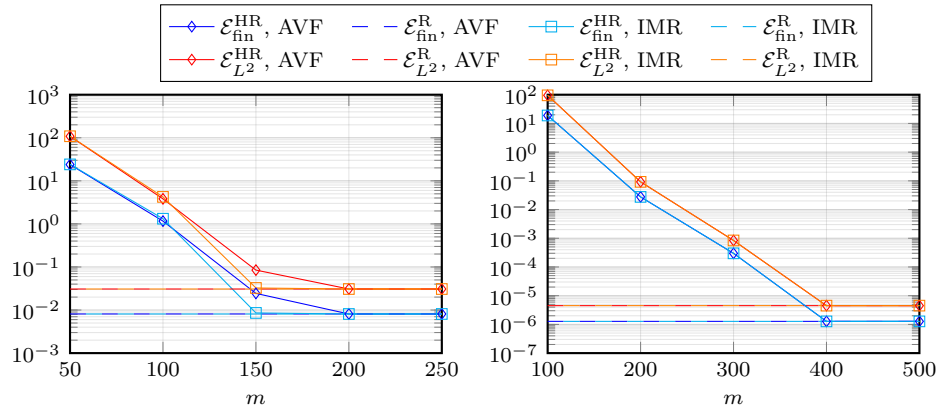


Figure 4: Schrödinger equation. Errors (5.1) of the reduced and hyper-reduced models vs. size m of the DEIM space. The size of the reduced model is $2k = 200$ (left) and $2k = 400$ (right). Comparison of AVF and IMR for time integration.

The computational time required to solve the reduced model and the hyper-reduced model online using the AVF time integration scheme are reported in Table 2. Similar results were recorded for the IMR timestepping. Combining the accuracy and the computational time, we observe that the error of the reduced model is reached by the hyper-reduced solution for $m = 200$ when $2k = 200$ in 27 seconds, and for $m = 400$ when $2k = 400$ in 2 minutes, with a reduction of a factor of 73 and of 17 with respect to the runtime of the reduced problem, respectively.

Table 2: Schrödinger equation. Computational times of the online phases of the reduced and hyper-reduced systems, $2k = 200$ (top) and $2k = 400$ (bottom). The test parameter is $\eta = 1.0932 \notin \Gamma_s$. AVF is used as time integrator. The reported times are computed as averages over 5 runs.

Reduced model $2k = 200$	$m = 50$	$m = 100$	$m = 150$	$m = 200$	$m = 250$
33 min	9.13 s	11.76 s	15.04 s	27.22 s	34.87 s
Reduced model $2k = 400$	$m = 100$	$m = 200$	$m = 300$	$m = 400$	$m = 500$
35 min	37.01 s	60.70 s	84.90 s	123.83 s	164.28 s

Concerning the conservation of the Hamiltonian, we perform a numerical analysis similar to the case of shallow water equations, see Section 5.1. We fix the size of the reduced model to $2k = 400$. In Figure 5 we report the evolution of the error in the conservation of the Hamiltonian $|\mathcal{H}(y^0) - \mathcal{H}(Az^j)|$,

for $j = 0, \dots, N_t$, together with the quantities involved in the bound (5.3). If AVF is used as time integrator (left plot), then $\varepsilon_{\mathcal{H}}^{[t^0, t^j]}$ is of the order of the tolerance of the nonlinear solver and the Hamiltonian error is dominated by the error $\Delta\mathcal{H}_j$ introduced with the DEIM hyper-reduction. If IMR is used as time integrator (right plot), the hyper-reduction error $\Delta\mathcal{H}_j$ decreases with m , but the error $\varepsilon_{\mathcal{H}}^{[t^0, t^j]}$ introduced by the time integration is dominant and there is no gain in increasing the size m of the DEIM basis.

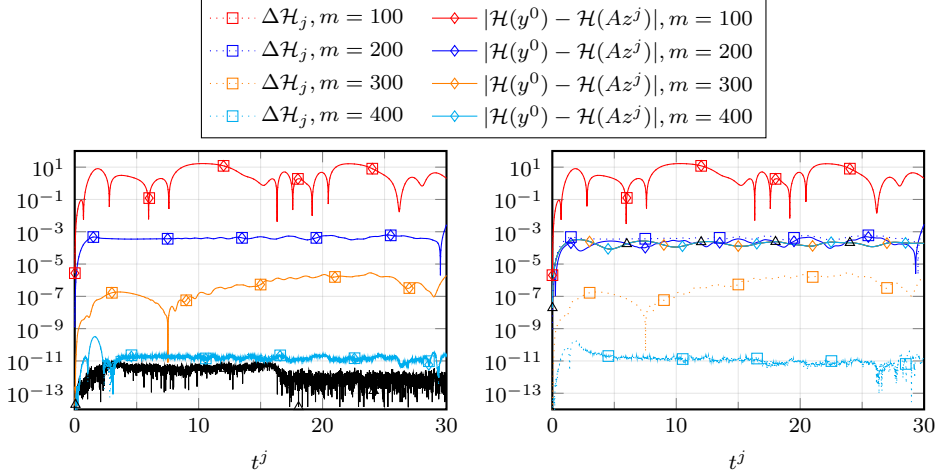


Figure 5: Schrödinger equation. Conservation of the Hamiltonian over time for different choices of the DEIM basis m . The solid black lines with triangular marks corresponds to the error $\varepsilon_{\mathcal{H}}^{[t^0, t^j]}$ of the full Hamiltonian due to the timestepping. AVF (left) and IMR (right) for time integration. The reduced model has dimension $2k = 400$ and the test parameter is $\eta = 1.0932 \notin \Gamma_s$.

Figure 6 confirms that the time evolution of $\Delta\mathcal{H}_j$ is determined by the accuracy of the DEIM approximation of the Hamiltonian.

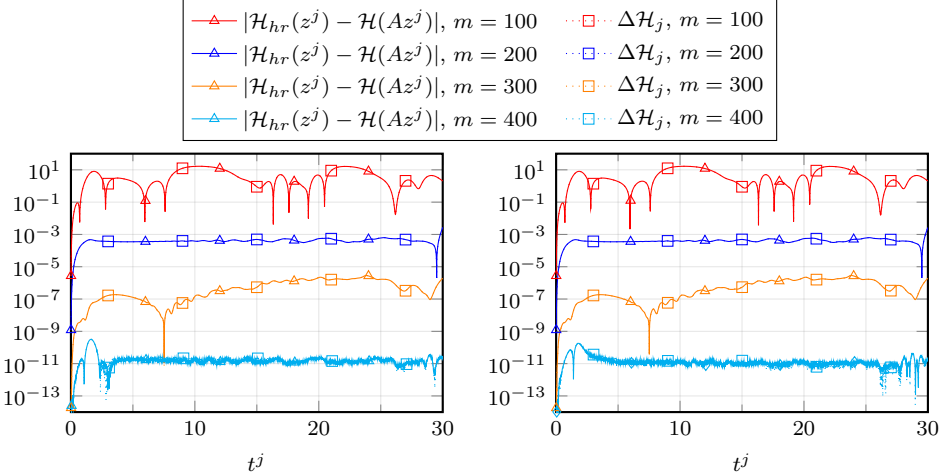


Figure 6: Evolution of the approximation error of Hamiltonian for different choices of the DEIM basis m . AVF (left) and IMR (right) for time integration. The reduced model has dimension $2k = 400$ and the test parameter is $\eta = 1.0932 \notin \Gamma_s$.

5.2.2 Adaptive hyper-reduction algorithm

From the previous numerical tests, it can be inferred that the dimension of the DEIM basis required by the hyper-reduced model to achieve the error of the reduced model is rather large, at least for this problem. For example, in Figure 4, one can observe that, for $2k = 400$, the hyper-reduced error reaches the target value of the reduced model error when $m \geq 400$, and it is still of order 1 when $m = 100$. This behavior can be ascribed to the fact that the Schrödinger equation and its Hamiltonian do not exhibit significant global reducibility properties. Figure 7 shows the singular values of the full order solution obtained for $N_t = 3000$ time steps and one value of the parameter, $\eta = 1.0932$. Figure 8 shows the singular values of the snapshot matrix $M_J \in \mathbb{R}^{n \times 2kN_s}$ of the Jacobian (3.6) for the same value of the parameter and for $N_s = 150$ time instants (one every 20 time steps). Each line corresponds to a different value of the dimension $2k$ of the reduced model. We can observe that the singular values of the snapshots corresponding to the full order solution decay relatively slowly (Figure 7), which suggests that the dimension $2k$ of the reduced space needs to be sufficiently large to accurately represent the full dynamics. On the other hand, the reducibility of the Jacobian deteriorates as $2k$ increases (Figure 8). This last remark also justifies our choice of performing hyper-reduction on the reduced Jacobian rather than on the full order one, as already pointed out in Remark 3.2.

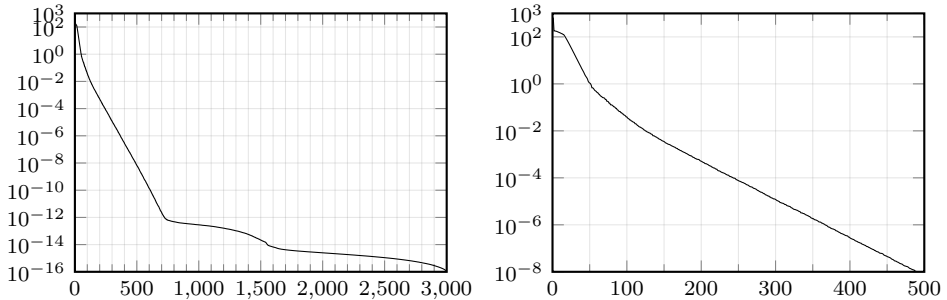


Figure 7: Schrödinger equation. Left: singular values of the snapshot matrix of the full order solution. Right: Zoom on the 500 largest singular values.

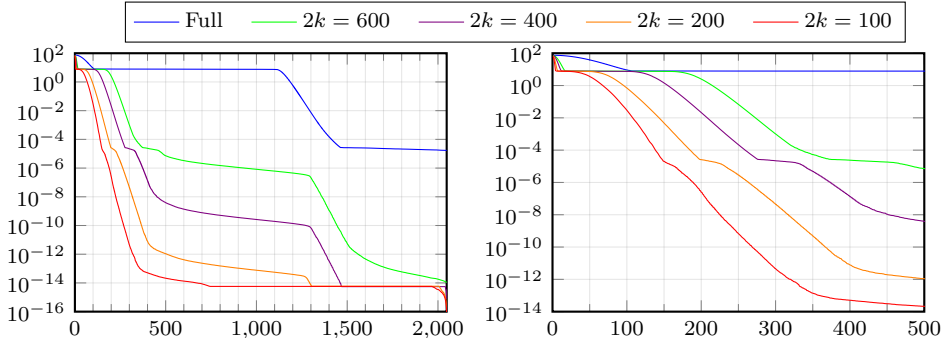


Figure 8: Schrödinger equation. Left: singular values of the snapshot matrix $M_J \in \mathbb{R}^{n \times 2N_s}$ of the Jacobian for different choices of k . Right: zoom on the 500 largest singular values for each case.

To address the lack of global reducibility of the Jacobian, we perform the adaptation of DEIM basis and indices described in Section 4. In this section we fix the size of the reduced basis to $2k = 400$.

As a first test, we consider, at each update step $j = 1, \dots, N_a$, the selection of the m_s sampling points collected in the matrix S_j and we compare three possible selection strategies: (i) random; (ii) based on the minimization of the residual norm $\|R_j\|_F$ as proposed in [20, Algorithm 1]; and

(iii) based on the minimization of the projected residual norm $\|R_j \mathbb{C}_j\|_F$ motivated by Theorem 4.3, see also Algorithm 2. We set the dimension of the DEIM basis to $m = 100$, while the adaptation hyper-parameters are $\delta = \delta_0 = \gamma = 5$, $w = 1$ and $r = \bar{r}$, namely a full-rank update is performed at each step. We compare the three selection strategies for two possible sizes of the sampling matrix, namely $m_s \in \{150, 300\}$. Figure 9 shows the error $\|U_{j+1} \mathbb{C}_j - F_j\|_F$, at each update j , for the three selection criteria.

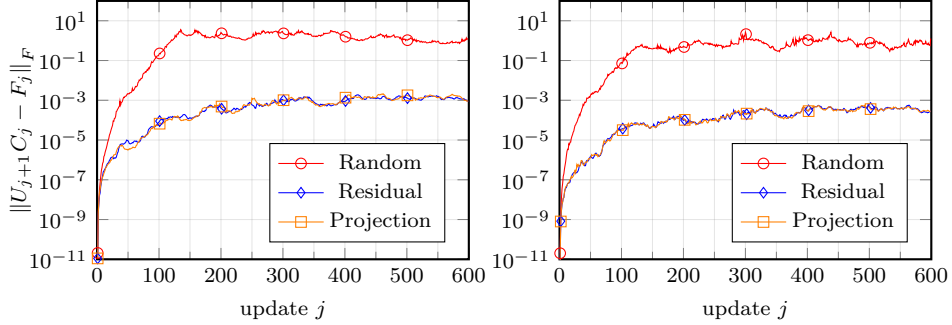


Figure 9: Schrödinger equation. Evolution of $\|U_{j+1} \mathbb{C}_j - F_j\|_F$ for three different criteria of selection of the sampling points. The hyper-parameters are $\delta = \delta_0 = \gamma = 5$, $w = 1$, $r = \bar{r}$. The number of sampling points is $m_s = 150$ (left plot) and $m_s = 300$ (right plot). The dimension of the reduced basis is $2k = 400$ and the dimension of the DEIM basis is $m = 100$.

The L^2 -errors (5.1) of the hyper-reduced solution with respect to the full order solution are reported in Table 3. It can be observed that the random algorithm gives worse results compared to the other two strategies, and that the other two strategies do not yield significantly different results, at least in this simulation.

Table 3: Schrödinger equation. Error $\mathcal{E}_{L^2}^{\text{HR}}$ obtained with the adaptive algorithm with three different criteria for the selection of the sampling points. The hyper-parameters are $\delta = \delta_0 = \gamma = 5$, $w = 1$, $r = \bar{r}$. The dimension of the reduced basis is $2k = 400$ and the dimension of the DEIM basis is $m = 100$.

$\mathcal{E}_{L^2}^{\text{HR}}$	Random	Residual	Projection
$m_s = 150$	5.1880e+01	1.1628e-02	1.2809e-02
$m_s = 300$	1.5281e+01	5.0569e-03	5.2635e-03

Next, we assess the adaptive hyper-reduction algorithm for different choices of the adaptation hyper-parameters – r , m_s , w , δ , and γ – in terms of: (i) accuracy of the solution, measured by the error $\mathcal{E}_{L^2}^{\text{HR}}$ from (5.1); and (ii) computational time of both the offline phase, t_{off} , and the online phase, t_{on} , computed as the average time, in seconds, over 5 independent runs. The sum of the two computational times is reported as t_{tot} .

In all the following tests, we fix the size of the DEIM basis to $m = 100$ and we let one hyper-parameter vary at a time. Based on the previous test and on the analysis in Section 4, the sampling strategy presented in Algorithm 2 is adopted for the update of the sampling indices.

As a reference, we include in our study the performances of the non-adaptive hyper-reduction, where the offline phase consists of the construction of the DEIM basis from the snapshot matrix M_J of the reduced Jacobian at the full model solutions obtained every 20 time steps and $|\Gamma_s| = 11$ training parameters. If the adaptive scheme is employed instead, the offline phase involves solving the full system for $\delta_0 \ll N_t$ time steps and only for the given test parameter. The snapshot matrix M_J of the reduced Jacobian only has $2k\delta_0$ columns instead of $2kN_s|\Gamma_s|$. Since $\delta_0 \ll N_s|\Gamma_s|$, the offline phase will only require few seconds; on the other hand, the DEIM basis is adapted every δ time steps, which increases the computational cost of the online phase with respect to the non-adaptive scheme. In the following experiments, we evaluate the computational cost of both phases and we compare the

adaptive and non-adaptive strategies by taking into account the overall runtime.

Effect of the rank r of the DEIM update. In a first test on the adaptive strategy, we assess the computational times and the error of the hyper-reduced model for different values of the rank r of the DEIM update, see Table 4. It can be observed that the error improves considerably as r increases, while the cost of the online phase of the adaptive hyper-reduction algorithm is almost independent of r . This is due to the fact that the cost of the adaptation procedure is dominated by the computation of the DEIM residual matrix R_j and the SVD of $R_j C_j$ in Algorithm 2, whose complexity is $O(dkmw)$, and thus independent of r .

It can also be observed that the error obtained with a rank $r = 50$ update is comparable to the one obtained with $r = m = 100$. Although for the optimality result of Lemma 4.2 a full-rank update is required, that is, $r_j = \bar{r}_j$ at every update step j , where $\bar{r}_j = \text{rank}(S_j^\top R_j C_j^\top) \leq m$, the results of Table 4 suggests that it might be enough to choose r equal to the numerical rank of $S_j^\top R_j C_j^\top$, by fixing a suitable tolerance.

Table 4: Error $\mathcal{E}_{L^2}^{\text{HR}}$ and computational times of the hyper-reduced model. Adaptive algorithm, effect of the update rank r .

		t_{off}	t_{on}	t_{tot}	$\mathcal{E}_{L^2}^{\text{HR}}$
Non-adaptive		152.77	38.52	191.29	9.5252e+01
$m_s = 250$	$r = 1$	5.47	54.52	59.99	7.4045e+01
$\delta_0 = \delta = 5$	$r = 10$	5.47	54.70	60.17	2.4352e+01
$w = 1$	$r = 20$	5.47	54.86	60.33	8.6444e-03
$\gamma = \delta$	$r = 50$	5.47	55.12	60.59	5.8579e-03
	$r = m = 100$	5.47	55.19	60.66	5.6615e-03

To confirm this observation, instead of fixing r we let it change at each update j based on the numerical rank of $S_j^\top R_j C_j^\top$ for a fixed tolerance τ_r . The rank r_j vs. the update number is shown in Figure 10 (left) for different choices of τ_r , while the error $\mathcal{E}_{L^2}^{\text{HR}}$ of the hyper-reduced solution is reported in Table 5. We observe that, in this experiment, there is no significant advantage in fixing the tolerance τ_r smaller than 10^{-8} and, correspondingly, performing a DEIM basis update of rank larger than 40. This is in accordance with the results of Table 4.

Table 5: Error $\mathcal{E}_{L^2}^{\text{HR}}$ and computational times of the hyper-reduced model. Adaptive algorithm, effect of the rank tolerance τ_r .

		t_{off}	t_{on}	t_{tot}	$\mathcal{E}_{L^2}^{\text{HR}}$
Non-adaptive		152.77	38.52	191.29	9.5252e+01
$m_s = 250$	$\tau_r = 10^{-4}$	5.44	54.83	60.27	2.7979e-01
$\delta_0 = \delta = 5$	$\tau_r = 10^{-6}$	5.44	55.17	60.61	9.9858e-03
$w = 1$	$\tau_r = 10^{-8}$	5.44	55.30	60.74	5.9148e-03
$\gamma = \delta$	$\tau_r = 10^{-10}$	5.44	55.46	60.90	5.6686e-03
	$\tau_r = 10^{-12}$	5.44	55.58	61.02	5.5454e-03

Effect of the number m_s of sampling points. We test the hyper-reduction algorithm for values of m_s in the set $\{100, 150, 200, 250, 300\}$, so that $m_s \geq m$ and $m_s \ll d$, see discussion after eq. (4.4). From Table 6, we can infer that, as m_s increases, the error can be drastically reduced.

Concerning the computational time, considerations similar to the case above (different values of the rank update) can be made: the cost is almost independent of the value of m_s , and the total time required by the adaptive algorithm is less than one third of the time needed by the non-adaptive algorithm. Even comparing online phases only, the adaptive scheme with DEIM size $m = 100$ and $m_s = 300$ sampling points takes roughly 5 seconds less than the non-adaptive case with $m = 200$, while the error is one order of magnitude smaller, see Figure 4 and Table 2.

Table 6: Error $\mathcal{E}_{L^2}^{\text{HR}}$ and computational times of the hyper-reduced model. Adaptive algorithm, effect of the number of sampling points m_s .

		t_{off}	t_{on}	t_{tot}	$\mathcal{E}_{L^2}^{\text{HR}}$
Non-adaptive		152.77	38.52	191.29	9.5252e+01
$\delta_0 = \delta = 5$	$m_s = 100$	5.74	54.75	60.49	3.6204e-02
	$m_s = 150$	5.74	54.88	60.62	1.2809e-02
$w = 1$	$m_s = 200$	5.74	55.14	60.88	7.1215e-03
	$m_s = 250$	5.74	55.05	60.79	5.6615e-03
$r = \bar{r}$	$m_s = 300$	5.74	55.06	60.80	5.2635e-03

Analogously to the rank of the update, instead of fixing m_s we may select the number of sampling indices on the basis of a tolerance τ_s . More precisely, an index is chosen at the j th adaptation step if the 2-norm of the corresponding row of $R_j \mathbb{C}_j$ is larger than τ_s . In this way, the number of sampling indices changes at each adaptation step and it is fixed to be at least equal to m . The results are reported in Table 7. The number of sampling indices selected at each adaptation for different choices of the tolerance is shown in Figure 10 (right).

Table 7: Error $\mathcal{E}_{L^2}^{\text{HR}}$ and computational times of the hyper-reduced model. Adaptive algorithm, effect of the sampling points tolerance τ_s .

		t_{off}	t_{on}	t_{tot}	$\mathcal{E}_{L^2}^{\text{HR}}$
Non-adaptive		152.77	38.52	191.29	9.5252e+01
$\delta_0 = \delta = 5$	$\tau_s = 10^{-2}$	5.50	54.66	60.16	3.6204e-02
	$\tau_s = 10^{-4}$	5.50	54.76	60.26	3.6204e-02
$w = 1$	$\tau_s = 10^{-6}$	5.50	54.81	60.31	3.6204e-02
	$\tau_s = 10^{-8}$	5.50	54.94	60.44	2.6294e-02
$r = \bar{r}$	$\tau_s = 10^{-10}$	5.50	55.66	61.16	5.5017e-03

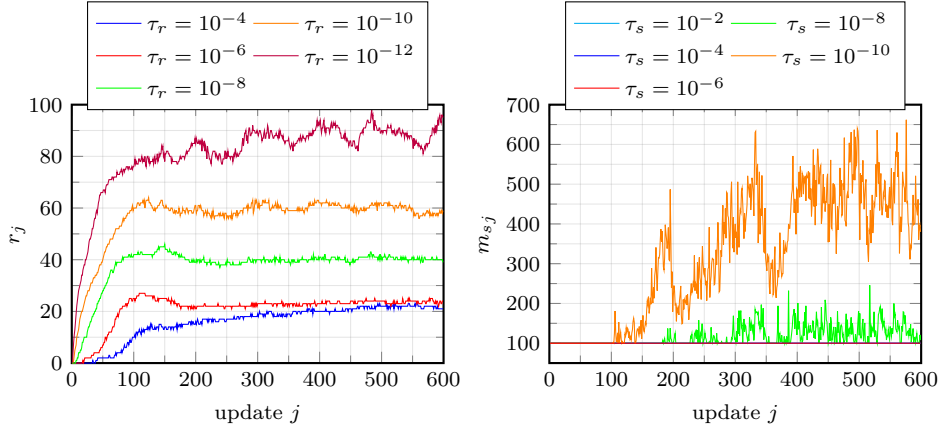


Figure 10: Schrödinger equation. Left: Rank $r_j = \text{rank}(S_j^\top R_j C_j^\top)$ at every update j for different values of the tolerance τ_r . Right: Number of sampling indices m_{sj} at every update j for different values of the tolerance τ_s .

Effect of the size w of the time window to evaluate the nonlinear term. The role of w in the adaptation is described in Section 4. In this test, we slightly increase the values of δ_0 and δ and set them equal to 10. The reason is that it must hold $w < \delta_0$, and, moreover, it is reasonable to require that $w < \delta$, that is, at each adaptation step, the temporal window only contains snapshots obtained after the last update. In Table 8 we observe that, as expected, the error $\mathcal{E}_{L^2}^{\text{HR}}$ decreases as more information from the past is included in the construction of the DEIM basis update. In parallel, the increase in the window size requires larger computational times in the online phase. However, it can be noticed that the online phase in the case $w = 1$ is only slightly more computationally expensive than the online phase of the non-adaptive algorithm, while the L^2 -error is reduced by almost four orders of magnitude.

Table 8: Error $\mathcal{E}_{L^2}^{\text{HR}}$ and computational times of the hyper-reduced model. Adaptive algorithm, effect of the window size w .

		t_{off}	t_{on}	t_{tot}	$\mathcal{E}_{L^2}^{\text{HR}}$
Non-adaptive		152.77	38.52	191.29	9.5252e+01
$m_s = 250$	$w = 1$	8.91	45.01	53.92	1.2007e-02
$\delta_0 = \delta = 10$	$w = 2$	8.91	50.82	59.73	1.0352e-02
$r = \bar{r}, \gamma = \delta$	$w = 4$	8.91	60.13	69.04	6.8395e-03
	$w = 6$	8.91	69.73	78.64	6.3531e-03

Effect of the number δ of time steps between each DEIM adaptation. Predictably, the online phase is cheaper for large δ since the adaptations are less frequent, while the error increases, as reported in Table 9.

Table 9: Error $\mathcal{E}_{L^2}^{\text{HR}}$ and computational times of the hyper-reduced model. Adaptive algorithm, effect of the number δ of time steps between each update of the DEIM basis.

		t_{off}	t_{on}	t_{tot}	$\mathcal{E}_{L^2}^{\text{HR}}$
Non-adaptive		152.77	38.52	191.29	9.5252e+01
$m_s = 250$	$\delta = 5$	5.55	55.05	60.60	5.6615e-03
$\delta_0 = 5, w = 1$	$\delta = 10$	5.55	46.40	51.95	1.2869e-02
$r = \bar{r}, \gamma = \delta$	$\delta = 20$	5.55	41.00	46.55	2.2929e-01

Effect of the number of time steps γ between each update of the sampling indices. In view of the discussion on the arithmetic complexity of Algorithm 2 in Section 4.2, it might seem preferable, in terms of computational cost, to update the sampling indices every $\gamma > 1$ time steps. Indeed, the larger γ , the less frequently Algorithm 2 is run, including the expensive computation of the full residual. In this test we consider $\gamma = \nu\delta$, meaning that the sampling points are updated every ν adaptations of the DEIM basis. We observe in Table 10 that the error $\mathcal{E}_{L^2}^{\text{HR}}$ in the hyper-reduced solution decreases each time γ is halved, with an increase in the runtime of the online phase of less than 5 seconds.

Table 10: Error $\mathcal{E}_{L^2}^{\text{HR}}$ and computational times of the hyper-reduced model. Adaptive algorithm, effect of the number γ of time steps between each update of the sampling indices.

	t_{off}	t_{on}	t_{tot}	$\mathcal{E}_{L^2}^{\text{HR}}$
Non-adaptive	152.77	38.52	191.29	9.5252e+01
$m_s = 250$	5.51	55.15	60.66	5.6615e-03
$\delta_0 = \delta = 5$	5.51	50.35	55.86	1.0154e-02
$w = 1$	5.51	48.20	53.71	7.8903e-02
$r = \bar{r}$	5.51	47.56	53.07	4.2094e-01

Although the behavior of the adaptive hyper-reduction algorithm under variation of the hyper-parameters is clearly problem-dependent, the numerical tests presented above suggest the following conclusions. The rank of the update r and the number m_s of sampling points affect the hyper-reduced model in a similar way: increasing them leads to a significant reduction of the error without any major effect on the computational time. On the other hand, the optimal values of r and m_s may depend on the adaptation step j and, hence, it seems preferable to let them vary in time according to a tolerance. The effect of w on the error is less evident: although the error decreases as w increases, the fast growth of the computational time t_{on} outweighs this gain. Finally, small values of δ and γ imply frequent adaptations of both the DEIM basis and sampling indices, and thus reduction in the error, at a mild increase of the computational cost of the simulation.

For the same combinations of hyper-parameters seen above, we study the conservation of the Hamiltonian in terms of the error $\Delta\mathcal{H}_{N_t} = |\mathcal{H}(y^{N_t}) - \mathcal{H}(Az^{N_t})|$. We refer to Proposition 4.4 for the analytic bound on the error, while we report in Table 11 the values of the terms appearing in the theoretical bound. When AVF is used as numerical time integrator, the error sources that are independent on the reduction give

$$\varepsilon_{\mathcal{H}}^{[t^0, t^{N_t}]} = 7.8160\text{e-}13 \quad \text{and} \quad \sum_{i=0}^{N_a-1} \varepsilon_{\mathcal{H}_{hr}^i}^{[t^{\ell_i}, t^{\ell_i+1}]} \leq 10^{-10}.$$

Therefore, we only record the error introduced by the jump terms

$$\sum_{i=1}^{N_a} |\mathcal{H}_{hr}^{i-1}(z^{\ell_i}) - \mathcal{H}_{hr}^i(z^{\ell_i})| \leq \sum_{i=1}^{N_a} \Delta(i-1, z^{\ell_i}) + \sum_{i=1}^{N_a} \Delta(i, z^{\ell_i}), \quad (5.5)$$

where $\Delta(i, z) := |\mathcal{H}(Az) - \mathcal{H}_{hr}^i(z)|$. In the numerical tests we do not enforce the condition $h(Az^{\ell_i}) \in \text{Col}(U_i)$ for any $i \geq 1$. This implies that the hypotheses of Proposition 4.4 are not satisfied. Nevertheless, as remarked at the end of Section 4.3, the two quantities on the right hand side of (5.5) typically have the same order of magnitude. This is confirmed by the numerical experiments as shown in Table 11. We remark that, in this set of numerical experiments, the bound on the Hamiltonian turns out to be rather pessimistic: this is due to the fact that the error $|\mathcal{H}_{hr}^0(z^0) - \mathcal{H}_{hr}^{N_a}(z^{N_t})|$ is

lower than the sum, for $i = 1, \dots, N_a$, of the jump terms $|\mathcal{H}_{hr}^{i-1}(z^{\ell_i}) - \mathcal{H}_{hr}^i(z^{\ell_i})|$, see the proof of Proposition 4.4.

Table 11: Schrödinger equation. Error in the Hamiltonian approximation at the final time and comparison with the terms of the bound in Proposition 4.4.

		$\sum_{i=1}^{N_a} \Delta(i-1, z^{\ell_i})$	$\sum_{i=1}^{N_a} \Delta(i, z^{\ell_i})$	$\Delta \mathcal{H}_{N_t}$
$m_s = 250$	$r = 1$	7.5797e+02	7.6869e+02	1.6115e+01
	$r = 10$	5.4406e+02	5.5495e+02	3.0423e+01
	$r = 20$	7.2296e-02	8.2476e-02	3.3438e-03
	$w = 1$	7.3965e-03	8.2384e-03	8.2357e-04
	$\gamma = \delta$	1.0716e-02	1.0901e-02	5.3122e-04
	$r = m = 100$			
$\delta_0 = \delta = 5$	$\tau_r = 10^{-4}$	4.4108e+00	4.9276e+00	7.0851e-02
	$\tau_r = 10^{-6}$	2.7979e-02	3.1075e-02	2.3695e-04
	$\tau_r = 10^{-8}$	7.3420e-03	8.0704e-03	6.8799e-04
	$w = 1$	7.0413e-03	7.8448e-03	8.0431e-04
	$\gamma = \delta$	6.5060e-03	7.2173e-03	7.2137e-04
	$\tau_r = 10^{-12}$			
$w = 1$	$m_s = 100$	1.6513e-01	1.7895e-01	1.1185e-02
	$m_s = 150$	4.1715e-02	4.3806e-02	2.0961e-03
	$m_s = 200$	1.5724e-02	1.6892e-02	1.3723e-03
	$r = \bar{r}$	1.0716e-02	1.0901e-02	5.3122e-04
	$\gamma = \delta$	1.4375e-02	1.4886e-02	4.9989e-04
	$m_s = 300$			
$r = \bar{r}$	$\tau_s = 10^{-2}$	1.6513e-01	1.7895e-01	1.1185e-02
	$\tau_s = 10^{-4}$	1.6513e-01	1.7895e-01	1.1185e-02
	$w = 1$	1.6513e-01	1.7895e-01	1.1185e-02
	$\gamma = \delta$	1.6513e-01	1.7895e-01	1.1185e-02
	$\tau_s = 10^{-6}$	5.7726e-02	6.3010e-02	5.1789e-03
	$\tau_s = 10^{-8}$	1.1946e-02	1.2198e-02	9.8049e-05
$\gamma = \delta$	$\tau_s = 10^{-10}$			
	$m_s = 250$	4.7735e-02	5.2877e-02	2.7434e-03
	$\delta_0 = \delta = 10$	1.5484e-02	1.8899e-02	9.3749e-04
	$r = \bar{r}, \gamma = \delta$	1.1988e-02	1.3121e-02	1.5510e-03
	$m_s = 250$	1.0716e-02	1.0901e-02	5.3122e-04
	$w = 1, \delta_0 = 5$	1.6424e-02	1.8540e-02	3.0796e-03
$w = 1$	$r = \bar{r}, \gamma = \delta$	1.9596e-01	2.9488e-01	4.9938e-02
	$m_s = 250$	1.0716e-02	1.0901e-02	5.3122e-04
	$\delta_0 = \delta = 5$	2.4803e-02	2.7459e-02	2.0355e-03
	$w = 1$	2.1990e-01	2.4045e-01	1.8280e-02
	$r = \bar{r}$	1.0649e+00	1.1809e+00	9.8951e-02
	$\gamma = 30$			

As a last numerical test, we fix the values of the hyper-parameters and compare the performances of the non-adaptive and adaptive hyper-reduction algorithms as the dimension m of the DEIM space varies. We set the hyper-parameters as follows: the tolerance in the choice of the update rank is $\tau_r = 10^{-12}$; the tolerance is the selection of the sampling points is $\tau_s = 10^{-20}$; the temporal window size is $w = 1$; the frequency of the updates is $\delta = \gamma = 5$.

In Figure 11 we report the error $\mathcal{E}_{L^2}^{\text{HR}}$ between the hyper-reduced solution and the full model solution vs. m (left plot) and vs. the algorithm runtime (right plot). The reported times are computed as averages over 5 runs.

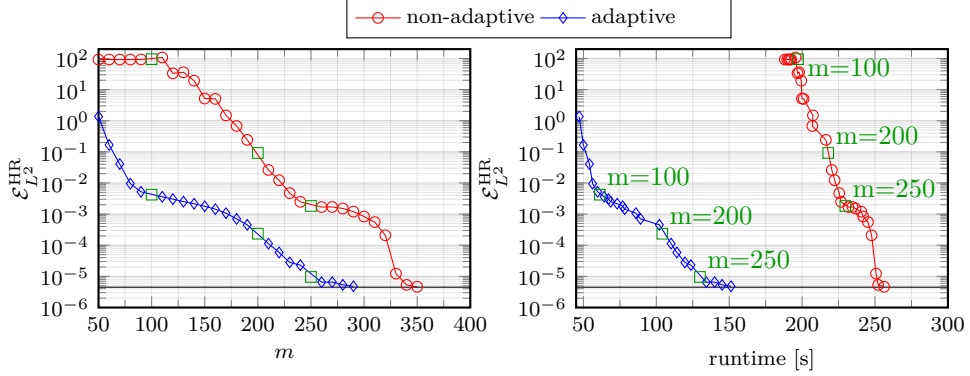


Figure 11: Schrödinger equation. Comparison between non-adaptive and adaptive hyper-reduction algorithms. Left: error $\mathcal{E}_{L^2}^{\text{HR}}$ vs. the DEIM size m . The black line represents the error $\mathcal{E}_{L^2}^R$ between the reduced solution and the full solution. Right: $\mathcal{E}_{L^2}^{\text{HR}}$ vs. the algorithm runtime t_{tot} for different values of m . The computational time to solve the reduced model is 2100s and, for better readability, it is not shown in the plot. The reduced model has size $2k = 400$.

The plot on the left of Figure 11 shows that, to achieve a given error, the adaptive scheme allows a smaller DEIM basis compared to the non-adaptive one. This translates in a reduced computational cost (right plot), despite the fact that the adaptive algorithm requires extra online operations to perform the DEIM update. This gain in the total computational time is also due to the fact that a more expensive online phase for adaptation is compensated by a cheaper offline phase compared to the non-adaptive strategy. As an example, the total computational cost is reduced by a factor 3 for $m = 100$, and by a factor 2 when $m = 200$. Moreover, for a given size m of the DEIM basis, the adaptive scheme yields smaller errors than the non-adaptive one: for example, the L^2 -error in the adaptive case is almost three orders of magnitude lower for $m = 200$. Finally, the hyper-reduced model achieves the error of the reduced model for $m = 290$ in the adaptive case, and for $m = 350$ in the non-adaptive one; for these values of m , the adaptive algorithm requires about 40% less runtime than the non-adaptive scheme.

6 Concluding remarks

We have proposed a hyper-reduction method to deal with large-scale parametric dynamical systems characterized by nonlinear gradient fields. Its combination with symplectic reduced basis methods enables efficient numerical simulations of Hamiltonian dynamical systems with general nonlinearities. Indeed the surrogate models resulting from the proposed hyper-reduction can be solved at a computational cost independent of the size of the full model and without compromising the physical properties of the dynamics thanks to the preservation of the gradient structure of the velocity field. Although we have focused on Hamiltonian dynamical systems, the method can be applied to any gradient field, appearing e.g. in gradient flows or in port-Hamiltonian problems.

Some questions remain open. A rigorous connection between the reducibility of the solution space, the reducibility of the space of nonlinear gradient fields and the reducibility of the space of reduced Jacobian matrices is not understood yet. This could provide useful insights on when the numerical

simulation of the dynamics of a certain system could significantly benefit from hyper-reduction and whether an adaptive approach is to be preferred over a global one.

Moreover, our hyper-reduction strategy hinges on the properties of the reduced space. We observe that a larger reduced space improves the approximation of the state but demands a larger DEIM basis to reach the same accuracy in the hyper-reduction of the nonlinear term. A natural idea to address this shortcoming is to consider symplectic reduced spaces that can evolve in time, as done e.g. in [19]. This would allow us to deal with small reduced spaces and hence highly reducible Jacobian matrices (i.e. small DEIM bases as well). The combination of evolving reduced spaces with adaptive hyper-reduction provides an interesting possible direction of future investigation.

Acknowledgment. CP would like to thank Benjamin Peherstorfer for several interesting discussions on adaptive DEIM.

References

- [1] B. M. Afkham and J. S. Hesthaven. “Structure preserving model reduction of parametric Hamiltonian systems.” *SIAM J. Sci. Comput.* 39.6 (2017), A2616–A2644.
- [2] M. Barrault, Y. Maday, N. C. Nguyen, and A. T. Patera. “An ‘empirical interpolation’ method: application to efficient reduced-basis discretization of partial differential equations.” *C. R. Math. Acad. Sci. Paris* 339.9 (2004), pp. 667–672.
- [3] P. Buchfink, A. Bhatt, and B. Haasdonk. “Symplectic model order reduction with non-orthonormal bases.” *Math. Comput. Appl.* 24.2 (2019), Paper No. 43, 26.
- [4] K. Carlberg, R. Tuminaro, and P. Boggs. “Preserving Lagrangian structure in nonlinear model reduction with application to structural dynamics.” *SIAM J. Sci. Comput.* 37.2 (2015), B153–B184.
- [5] E. Celledoni, V. Grimm, R. I. McLachlan, D. I. McLaren, D. O’Neale, B. Owren, and G. R. W. Quispel. “Preserving energy resp. dissipation in numerical PDEs using the “average vector field” method.” *J. Comput. Phys.* 231.20 (2012), pp. 6770–6789.
- [6] S. Chaturantabut, C. Beattie, and S. Gugercin. “Structure-preserving model reduction for nonlinear port-Hamiltonian systems.” *SIAM J. Sci. Comput.* 38.5 (2016), B837–B865.
- [7] S. Chaturantabut and D. C. Sorensen. “Nonlinear model reduction via discrete empirical interpolation.” *SIAM J. Sci. Comput.* 32.5 (2010), pp. 2737–2764.
- [8] S. Chaturantabut and D. C. Sorensen. “A state space error estimate for POD-DEIM nonlinear model reduction.” *SIAM J. Numer. Anal.* 50.1 (2012), pp. 46–63.
- [9] Z. Drmač and S. Gugercin. “A new selection operator for the discrete empirical interpolation method—improved a priori error bound and extensions.” *SIAM J. Sci. Comput.* 38.2 (2016), A631–A648.
- [10] C. Farhat, T. Chapman, and P. Avery. “Structure-preserving, stability, and accuracy properties of the energy-conserving sampling and weighting method for the hyper reduction of nonlinear finite element dynamic models.” *Internat. J. Numer. Methods Engrg.* 102.5 (2015), pp. 1077–1110.
- [11] Y. Gong, Q. Wang, and Z. Wang. “Structure-preserving Galerkin POD reduced-order modeling of Hamiltonian systems.” *Comput. Methods Appl. Mech. Engrg.* 315 (2017), pp. 780–798.
- [12] T. H. Gronwall. “Note on the derivatives with respect to a parameter of the solutions of a system of differential equations.” *Ann. of Math. (2)* 20.4 (1919), pp. 292–296.
- [13] E. Hairer, C. Lubich, and G. Wanner. *Geometric numerical integration*. Second. Vol. 31. Springer Series in Computational Mathematics. Springer-Verlag, Berlin, 2006.
- [14] N. Halko, P. G. Martinsson, and J. A. Tropp. “Finding Structure with Randomness: Probabilistic Algorithms for Constructing Approximate Matrix Decompositions.” *SIAM Review* 53.2 (2011), pp. 217–288.
- [15] J. S. Hesthaven and C. Pagliantini. “Structure-preserving reduced basis methods for Poisson systems.” *Math. Comp.* 90.330 (2021), pp. 1701–1740.
- [16] B. Kramer and K. E. Willcox. “Nonlinear model order reduction via lifting transformations and proper orthogonal decomposition.” *AIAA J.* 57.6 (2019), pp. 2297–2307.
- [17] S. Lall, P. Krysl, and J. E. Marsden. “Structure-preserving model reduction for mechanical systems.” *Phys. D* 184.1-4 (2003), pp. 304–318.

- [18] J. E. Marsden and T. S. Ratiu. *Introduction to mechanics and symmetry*. Second. Vol. 17. Texts in Applied Mathematics. Springer-Verlag, New York, 1999.
- [19] C. Pagliantini. “Dynamical reduced basis methods for Hamiltonian systems.” *Numer. Math.* 148.2 (2021), pp. 409–448.
- [20] B. Peherstorfer. “Model reduction for transport-dominated problems via online adaptive bases and adaptive sampling.” *SIAM J. Sci. Comput.* 42.5 (2020), A2803–A2836.
- [21] B. Peherstorfer and K. Willcox. “Online adaptive model reduction for nonlinear systems via low-rank updates.” *SIAM J. Sci. Comput.* 37.4 (2015), A2123–A2150.
- [22] L. Peng and K. Mohseni. “Symplectic model reduction of Hamiltonian systems.” *SIAM J. Sci. Comput.* 38.1 (2016), A1–A27.
- [23] A. Quarteroni, A. Manzoni, and F. Negri. *Reduced basis methods for partial differential equations*. Vol. 92. Unitext. Springer, Cham, 2016.
- [24] G. R. W. Quispel and D. I. McLaren. “A new class of energy-preserving numerical integration methods.” *J. Phys. A* 41.4 (2008), pp. 045206, 7.
- [25] S. Sultana and Z. Rahman. “Hamiltonian formulation for water wave equation.” *Open Journal of Fluid Dynamics* 3.2 (2013), pp. 75–81.
- [26] Z. Wang. *Structure-Preserving Galerkin POD-DEIM Reduced-Order Modeling of Hamiltonian Systems*. 2021. arXiv: [2103.00388](https://arxiv.org/abs/2103.00388).